An Analytic Method of Propagating a Covariance Matrix to a Maneuver Condition for Linear Covariance Analysis During Rendezvous

by

Capt Jesse Ross Gossner

B.S.A.E., United States Air Force Academy

(1981)

Submitted in Partial Fulfillment
of the Requirements for the
Degree of

Master of Science

in Aeronautics and Astronautics

at the

Massachusetts Institute of Technology

June, 1991

Signature of Author _____

Department of Aeronautics and Astronautics
June, 1991

Certified by _____

Professor Richard H. Battin
Department of Aeronautics and Astronautics
Thesis Supervisor

Certified by _____

Peter M. Kachmar
Technical Supervisor, CSDL

Certified by _____

Stanley W. Shepperd
ical Supervisor, CSDL

Accepted by _____

Professor Harold Y. Wachman
Chairman, Departmental Graduate Committee

An Analytic Method of Propagating a Covariance Matrix to a Maneuver Condition for Linear Covariance Analysis During Rendezvous

by
Capt Jesse Ross Gossner

Submitted to the
Department of Aeronautics and Astronautics
on May 15, 1991 in partial fulfillment of the requirements
for the Degree of Master of Science.

ABSTRACT

This study develops a method for analytically propagating a covariance matrix to a maneuver condition to be used in linear covariance analysis for planning the rendezvous phase of a space mission. With the generalized formulation of a condition transition matrix, an analytic method of propagating an augmented covariance matrix to any scalar terminal maneuver condition is presented. The twenty-six dimensional augmented covariance matrix used in this study includes navigation state errors, state dispersions, and time errors for both the chaser and target craft.

The method is, first, analytically developed. The vehicles are brought to the desired rendezvous condition by linearizing the motion at the maneuver condition point and allowing the time of flight to vary slightly. The analytic propagation technique is then validated by comparison to a stochastic Monte Carlo simulation for the case of several elevation angle conditions which might be used to trigger an initial rendezvous intercept burn. The validity of linearizing the motion about the terminal point is substantiated with the same simulation.

Thesis Supervisor: Dr. Richard H. Battin
Title: Adjunct Professor of Aeronautics and Astronautics

Technical Supervisor: Peter M. Kachmar
Title: Section Chief, The Charles Stark Draper Laboratory, Inc.

Technical Supervisor: Stanley W. Shepperd
Title: Staff Engineer, The Charles Stark Draper Laboratory, Inc.

ACKNOWLEDGEMENTS

This study has been made possible through the help and support of many people and organizations. I offer my thanks to the Draper Laboratory, the Air Force Institute of Technology, and the Massachusetts Institute of Technology.

The people of these organizations were outstanding in their professionalism, support and friendship. To Dr. Battin for your enthusiastic instruction in, and love for, Astrodynamics. To Liz Zotos for keeping me out of trouble at MIT. To John Sweeney and Tim Brand for making this Fellowship available. To Pete Kachmar for presenting the problem and for wisdom in solving it. To Stan Shepperd for pointing me in the right direction and nudging me when I got stuck. To Matt Bottkol for your mathematical expertise. To Bill Chu for sharing your knowledge of the main frame, JCL, and HAL. To Barbara and Lori for your secretarial support. To Vicki for a contract number and, more importantly, a charge account number. ...Thank You!

Many special friends served to make this time memorable. Special thanks to Carole Jablonski, my homework buddy, and Paul DiDomenico, my across the hall buddy and special friend. And to the gang of fellows and ex-fellows, Thank You.

Beside every great woman, stands a man (isn't that how it goes?). My wife, Susan, is truly great. I am privileged to share her love and companionship. Thank You!

Finally, and most importantly, I thank God. After all, he wrote the laws we try so hard to figure out.

This report was prepared at The Charles Stark Draper Laboratory, Inc. under NASA Contract # NAS9-18147.

Publication of this report does not constitute approval by the Draper Laboratory or the sponsoring agency of the findings or conclusions contained herein. It is published for the exchange and stimulation of ideas.

I hereby assign my copyright of this thesis to The Charles Stark Draper Laboratory, Inc., Cambridge, Massachusetts.

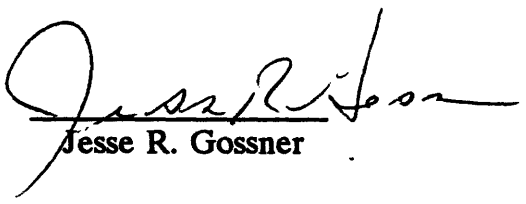

Jesse R. Gossner

Permission is hereby granted by The Charles Stark Draper Laboratory, Inc., to the Massachusetts Institute of Technology to reproduce any or all of this thesis.

TABLE OF CONTENTS

LIST OF FIGURES

LIST OF TABLES

LIST OF SYMBOLS

Symbol	Description
E[*]	Expected Value of *
$\boldsymbol{E}$	Covariance Matrix
Φ_T	Time transition matrix
Φ_C	Condition transition matrix
Φ_I	Idempotent transition matrix
$\boldsymbol{I}$	Identity matrix
$\mathbf{0}$	Null vector or matrix
$\boldsymbol{r}$	Position vector
$\boldsymbol{v}$	Velocity vector
$\Delta\boldsymbol{r}$	Relative position vector
$\boldsymbol{x}$	State vector
$\dot{\boldsymbol{x}}$	Time derivative of the state vector
$\boldsymbol{k}^{\mathrm{T}}$	Sensitivity vector
$\delta\boldsymbol{x}$	True Dispersion vector
$\boldsymbol{e}$	Navigation error vector
$\delta\hat{\boldsymbol{x}}$	Estimated Dispersion vector
$\boldsymbol{h}$	Angular momentum vector

δt	Time dispersion
ω	Orbital angular velocity
$\dot{\gamma}$	Time derivative of the flight path angle
μ	Gravitational parameter
ξ	Arbitrary maneuver condition
ϕ	Elevation angle maneuver condition

Subscript

c	Chaser vehicle
t	Target vehicle
s	Slip, change in time of flight
i	Matrix or vector at initial time
f	Matrix or vector propagated to final time
C	Matrix or vector propagated to condition constraint
A	Augmented matrix or vector
#	Indicates dimension of vector or square matrix
nom	Nominal state
true	True state
nav	Navigation state
pert	Perturbed state

Acronym

UVW	U, V, W coordinate system
LVC	Local vertical, curvilinear coordinate system
LOS	Line of sight coordinate system

Number Convention

Scalar	Normal text
Vector	Lower case, bold text
Matrix	Upper case, bold text

CHAPTER 1
INTRODUCTION

The purpose of this study is to develop an analytic method for propagating a covariance matrix to a maneuver condition to be used in linear covariance analysis for planning the rendezvous phase of a space mission. Rendezvous performance analysis usually includes the use of linear covariance and deterministic simulation techniques. Most rendezvous profiles include maneuvers to conditions (eg.: the position of the chaser craft relative to the target), as well as the more standard maneuvers to a fixed time. This study presents an analytic method of propagating the covariance matrix to a condition other than time.

This chapter motivates and introduces the subject: Section 1.1 provides the motivation for developing the method, Section 1.2 details a brief background of the current approach to propagating to an elevation angle condition, Section 1.3 discusses previous work that forms a starting point for this study, and Section 1.4 overviews the remaining chapters.

1.1 Motivation

Future missions to Mars will stretch current theories and practices in mission planning and operations well beyond those used to go to the moon. Several factors serve to greatly complicate the problem. Probably the greatest complicating factor is the distance involved. Because of the distance, most operations in the vicinity of Mars will need to be autonomous. Recent mission architectures, whether manned or robotic, have pointed to a need for an elliptic rendezvous capability. Great fuel savings can be gained by leaving the heavy interplanetary ship in a high energy elliptic orbit. The cost of taking only the landing craft down to a lower orbit and/or the surface, and then lifting it back to the high energy orbit would be much smaller than the cost of putting the interplanetary ship in a low circular orbit. This mission scenario, coupled with the remoteness of Mars, leads to a more complicated rendezvous problem than the near circular rendezvous typical of Apollo and current Space Shuttle operations.

Some of the questions that need to be re-addressed in an elliptic rendezvous problem are [3]:

- the shape and size of the catch-up orbit,
- where in the orbit the rendezvous should be initiated,
- the condition on which to trigger the intercept burn,
- where in the orbit the rendezvous should occur,
- the geometry of the final approach to the target, and
- whether the rendezvous scheme can be made tolerant of navigation uncertainties.

All these questions are interrelated, and, clearly, some trade-offs will have to be made. Near circular rendezvous experience provides a starting point, but complications, like the orbital velocity vector no longer being aligned, essentially, in the horizontal direction, may dictate different solutions than those currently used for near circular orbits.

Because of the trade-offs involved, mission planning is an iterative process. The analytic method set forth in this study was devised to simplify and increase the accuracy of the search for answers to these questions during the mission planning phase by providing an analytic method of propagating the covariance matrix to a condition. While the method of propagating to a condition will be completely general, this study will focus on observable conditions which might be used as the trigger point for the intercept burn.

1.2 Background

Presently, the condition used to trigger the intercept burn for co-circular rendezvous profiles and for reducing approach trajectory dispersions for shuttle rendezvous operations is the elevation angle of the line of sight from the chaser to the target craft, measured from the chaser's local horizontal. If the elevation angle is held constant, then for all dispersed trajectories, state errors perpendicular to the line of sight between the spacecraft will be zero at the condition. The current method of propagating a covariance matrix to this condition uses an empirical approach. The matrix is first extrapolated to the time at which the nominal orbit meets the condition. It is, then, empirically 'shaped' so the covariance reflects the zero error condition perpendicular to the line of sight and the resulting dispersions

that exist at the condition as seen from deterministic simulations. Monte Carlo simulation results confirm this method is essentially equivalent to extrapolating to the condition. This study seeks to find an analytic method of extrapolation to the condition by allowing for the possibility of time slips which are necessary to meet the condition in the presence of errors.

1.3 Previous Work

Two previous studies were reviewed which deal with developing a transition matrix which propagates an error vector to a condition rather than through a fixed time of flight. This section briefly describes each one.

Shepperd develops a method for directly determining the six dimensional transition matrix corresponding to any conic state extrapolation problem [6]. His method assumes a general form for the variation of the conic constraint equation with three unknown functional coefficients. He then derives the state transition matrix in terms of these three unknown functions, which are different for each conic problem. His structure is formulated in terms of Goodyear's universal variables. After presenting a completely general method for computing the state transition matrix for an arbitrary conic extrapolation problem, he demonstrates the derivation of the three functions for the most commonly encountered single craft constraints; extrapolation through a fixed time, or through a central angle, and extrapolation to a terminal radius. The advantage of this method is that, in general, Kepler's equation need not be solved, nor is it necessary to determine the time transition matrix.

Tempelman takes a different approach, starting with the six dimensional time

transition matrix and then allowing the time of flight to vary [10]. By assuming linear motion at the terminal point, the vehicle is constrained to either a traverse or a terminal cutoff condition with small variations in the final time. An associated time partial which defines the change in the time of flight is developed for each condition. Tempelman's method is also completely general, making use of sensitivity vectors, which are the partial derivatives of the desired cutoff condition with respect to the final and initial state vectors. He, too, demonstrates the derivation of the sensitivity vectors for several common single craft traverse and terminal constraints. Tempelman's approach is the starting point for this study because of its inherent simplicity and versatility in handling a multitude of problems. The development of Section 2.3.1 parallels his work in ref. [10].

1.4 Thesis Overview

This study develops a generalized condition transition matrix for a different class of constraints; maneuver conditions concerned with the relative position of a chaser and target spacecraft during rendezvous.

Chapter 2 presents the analytic development. First, the time transition matrix is augmented in three ways:

- Time is added to the state, so that the time partial is incorporated into the final condition transition matrix.
- The state is expanded to include both the chaser and target vehicles.
- The perturbation state is further expanded to included navigation errors and guidance dispersions.

The augmented condition transition matrix is then derived with the help of the

sensitivity vector. Finally, the derivation of the sensitivity vector is demonstrated for several elevation angle conditions.

A simulation is presented in Chapter 3, which compares the analytic results to a stochastic Monte Carlo simulation. The simulation was written to validate the analytic development and to gain some insight into the size of perturbations that can be introduced without exceeding the region of linearity at the terminal point. The key components of the simulation (the error generator, Monte Carlo, and the Analytic routine) are described in some detail.

Chapter 4 presents the results of the simulation. Key findings are made to support the validity of the analytic development and the linearity assumption. Two coordinate transformations are used to show the effect of the linearity assumption on the final perturbations and to help 'see' what the constrained perturbations 'look' like at the maneuver condition.

Conclusions drawn from the results of the simulation are summarized in Chapter 5. Lessons learned from this study are presented, and topics for future research are mentioned.

CHAPTER 2
ANALYTIC DEVELOPMENT

For certain rendezvous mission architectures, when the primary goal is to bring two spacecraft together, the actual time that certain events or conditions occur takes on less importance than the fact that they do occur at some point in the relative trajectory. In this case, the time of flight of a perturbed trajectory is allowed to vary from the nominal to ensure that the condition is still met in the presence of errors. While several different conditions may be utilized during the course of a rendezvous, the primary condition of interest in this study is the elevation angle of the line of sight to the target with respect to either the chaser's local horizontal or its velocity vector. This provides a unique scalar condition to be met at the terminal condition point.

This chapter takes these conditions and develops an analytic method of propagating a covariance matrix to satisfy any such condition. Section 2.1 shows how the covariance matrix is propagated, Section 2.2 defines the individual members of the state, and Section 2.3 develops the condition transition matrix.

2.1 Propagating to a Condition

The normal method of covariance matrix propagation uses the time transition matrix, Φ_T. Just as this transition matrix takes an error vector through a fixed time of flight, it can be used to propagate the covariance matrix through the same fixed time of flight:

$$E_f = \Phi_T E_i \Phi_T^T \tag{2.1}$$

where E is the covariance matrix and the subscripts i and f designate the initial and final points on the nominal trajectory.

The same idea works for propagating to some other scalar condition. If we can find a time varying condition transition matrix, Φ_C, which takes an error vector to a given condition while allowing the time of flight to vary, the same pre- and post-multiplication will propagate the initial covariance matrix to this condition:

$$E_C = \Phi_C E_i \Phi_C^T \tag{2.2}$$

Deriving a method to find this condition transition matrix is the primary goal of this chapter.

2.2 Defining the State and the Time Transition Matrix

Before we can find a condition transition matrix, we must, first, define the elements of the state vector we wish to propagate. This will also lead to the

appropriate time transition matrix, another necessary ingredient. The starting point is the traditional six dimensional state of one craft including three components of position and three of velocity. The errors in this state are then defined as: $\delta x = [\delta r , \delta v]$.

2.2.1 Adding Time to the State

Because we are going to allow time to slip to meet the terminal condition, we need to keep track of this slip. The easiest way to do this is to add time to the state. This time 'error' will be defined as the difference between the time the perturbed state achieves the condition, and the time the nominal state achieves the condition. In most cases, the initial time error will be zero, but it is conceivable to have an initial error resulting from a prior time slip or simply a small difference between the actual and nominal state update times.

For a first look, the equation for propagating errors with the six dimensional time transition matrix is used, assuming a constant time of flight. The equation for propagating the six dimensional state and a simple equation for time can then be combined to define a larger state and time transition matrix.

$$\begin{aligned} \delta x_f &= \Phi_T \delta x_i \\ \delta t_f &= \delta t_i \end{aligned} \quad \rightarrow \quad \begin{bmatrix} \delta x_f \\ \delta t_f \end{bmatrix} = \begin{bmatrix} \Phi_T & 0_6 \\ 0_6^T & 1 \end{bmatrix} \begin{bmatrix} \delta x_i \\ \delta t_i \end{bmatrix} \tag{2.3}$$

where 0_6 is a six dimensional null vector. Notice that any initial time error is just passed through to the final state. In this case, because the time of flight is kept constant, there is no change in the time error and this error has no effect on the rest of the state.

Taking this formulation one step further, a small time slip, δt_s^*, is introduced by linearizing the motion at the terminal point.

$$\begin{aligned} \delta x_f &= \Phi_T \delta x_i + \dot{x}_f \delta t_s^* \\ \delta t_f &= \delta t_i + \delta t_s^* \end{aligned} \quad \rightarrow \quad \begin{bmatrix} \delta x_f \\ \delta t_f \end{bmatrix} = \begin{bmatrix} \Phi_T & 0 \\ 0^T & 1 \end{bmatrix} \begin{bmatrix} \delta x_i \\ \delta t_i \end{bmatrix} + \begin{bmatrix} \dot{x}_f \\ 1 \end{bmatrix} \delta t_s^* \qquad (2.4)$$

where $\dot{x}$ is the first derivative of the nominal state (referred to as the dynamical state by Tempelman). For conic motion, $\dot{x} = [v, a]$, the craft's velocity and acceleration vectors, with $a = -\mu r/r^3$. The time slip is arbitrary for the moment, but will provide the degree of freedom needed to satisfy some, as yet unspecified, scalar constraint condition.

However, for rendezvous, two state vectors must be considered. Furthermore, not only would we like to have the two craft get together or at least arrive at a specified relative condition, but we need this event to occur at the same time for both craft. That means the final time error for the chaser must equal the final time error for the target. Since the two craft could have different initial time errors, we need some way to ensure they end up at the condition with the same clock time. While we could plan on having a different time slip for each craft to account for any initial time differences, an easier and more straight-forward solution is to convert initial time errors into initial position and velocity errors. Then, because this initial time error is 'absorbed' by the rest of the initial state, it makes no contribution to the final time error. As a result, an equal time slip for both craft to meet the terminal condition requirement will give us equal final time errors, as required.

In ref. [9], Tempelman shows how this might be done. The basic idea is that

since the time slip is arbitrary at this point, no generality is lost if a bias is introduced. Thus, defining:

$$\delta t_s^* = \delta t_s - \delta t_i \tag{2.5}$$

where δt_s is a new time slip and δt_i is the bias. Introducing this change of variables into equation (2.4) yields:

$$\begin{aligned} \delta x_f &= \Phi_T \delta x_i + \dot{x}_f (\delta t_s - \delta t_i) \\ \delta t_f &= \delta t_i + (\delta t_s - \delta t_i) = \delta t_s \end{aligned} \quad \Rightarrow \quad \begin{bmatrix} \delta x_f \\ \delta t_f \end{bmatrix} = \begin{bmatrix} \Phi_T & -\dot{x}_f \\ 0_6^T & 0 \end{bmatrix} \begin{bmatrix} \delta x_i \\ \delta t_i \end{bmatrix} + \begin{bmatrix} \dot{x}_f \\ 1 \end{bmatrix} \delta t_s \tag{2.6}$$

This result is basically the same as equation (2.4) except that this initial time slip error has been absorbed into the state vector part of the extrapolation. Instead of propagating the initial state errors a fixed time of flight and leaving them at a perturbed time, the errors are propagated by the same time of flight and then 'flown' back to the nominal time. Then, in both cases, they are propagated to whatever time slip is required to meet the terminal condition. Because the final time error is equal to the time slip, both craft will be on the same clock.

Note the seven dimensional time transition matrix is now singular, which only means we cannot go backward in time and separate the initial time error from the initial position and velocity errors. They are joined for good. Fortunately, this is not a problem.

2.2.2 Two Vehicles

At this point, we are confronted with the task of rendezvousing two spacecraft, each with its own uncertain state, modeled as a nominal state and a

covariance matrix. Much of current literature simplifies the problem by either assuming perfect knowledge of the target, or grouping the uncertainty of both craft into the chaser's covariance matrix. The time slip is then propagated along a relative trajectory which is the difference between the dynamical states of the chaser and the target ($\dot{x}_r = \dot{x}_c - \dot{x}_t$). In either case, the effect is the replacement of two full state vectors by the single relative state vector which leads to suboptimal performance.

In the Mars environment, with errors likely to be larger, this approximation may not be acceptable. We, therefore, keep all the information available by augmenting the state to include both vehicles.

$$\begin{aligned} \delta x_{c_f} &= \Phi_{T_c} \delta x_{c_i} - \dot{x}_{c_f} \delta t_{c_i} + \dot{x}_{c_f} \delta t_s \\ \delta x_{t_f} &= \Phi_{T_t} \delta x_{t_i} - \dot{x}_{t_f} \delta t_{t_i} + \dot{x}_{t_f} \delta t_s \qquad \rightarrow \\ \delta t_{c_f} &= \delta t_{t_f} = \delta t_s \end{aligned}$$

$$\delta x_A = \begin{bmatrix} \delta x_c \\ \delta x_t \\ \delta t_c \\ \delta t_t \end{bmatrix} \qquad \dot{x}_A = \begin{bmatrix} \dot{x}_c \\ \dot{x}_t \\ 1 \\ 1 \end{bmatrix} \qquad \Phi_A = \begin{bmatrix} \Phi_{T_c} & 0_{6x6} & -\dot{x}_{c_f} & 0_6 \\ 0_{6x6} & \Phi_{T_t} & 0_6 & -\dot{x}_{t_f} \\ 0_6^T & 0_6^T & 0 & 0 \\ 0_6^T & 0_6^T & 0 & 0 \end{bmatrix} \tag{2.7}$$

$$\delta x_{A_f} = \Phi_A \delta x_{A_i} + \dot{x}_{A_f} \delta t_s$$

where the subscripts c and t designate chaser and target, and A designates the augmented states and time transition matrix. Note that the basic equation is

unchanged.

2.2.3 Errors and Dispersions

Covariance analysis often involves the use of two basic types of perturbations. Navigation errors, or just errors, are the difference between the navigation, or estimated, state and the actual state of the vehicle. These errors develop from imperfect navigation measurements which are used by a Kalman filtering system to estimate position and velocity. When formulated as a covariance matrix, they represent the uncertainty of the navigation estimate. Dispersions, on the other hand, are the difference between the vehicle's actual state and the nominal, or planned, state. They are the result of imperfect maneuver execution and the use of linearized guidance laws or imperfect gravity models during a mission. As the vehicle tries to proceed along its nominal trajectory, small errors in the time of execution of a maneuver or the direction or duration of a burn cause the vehicle to deviate from the nominal trajectory. In a covariance matrix formulation, the dispersions represent the space about a point on the nominal trajectory where the vehicle should actually be. The estimated (navigation) dispersion from nominal is the sum of the state error and the actual dispersion.

$$
\begin{aligned}
x_{true} &= x_{nom} + \delta x \\
x_{nav} &= x_{nom} + \delta x + e \\
&= x_{nom} + \delta \hat{x} \\
&= x_{true} + e
\end{aligned}
\tag{2.8}
$$

where x is the six dimensional state of position and velocity with subscripts designating the nominal, true, and navigation states, δx is now the dispersion, e is

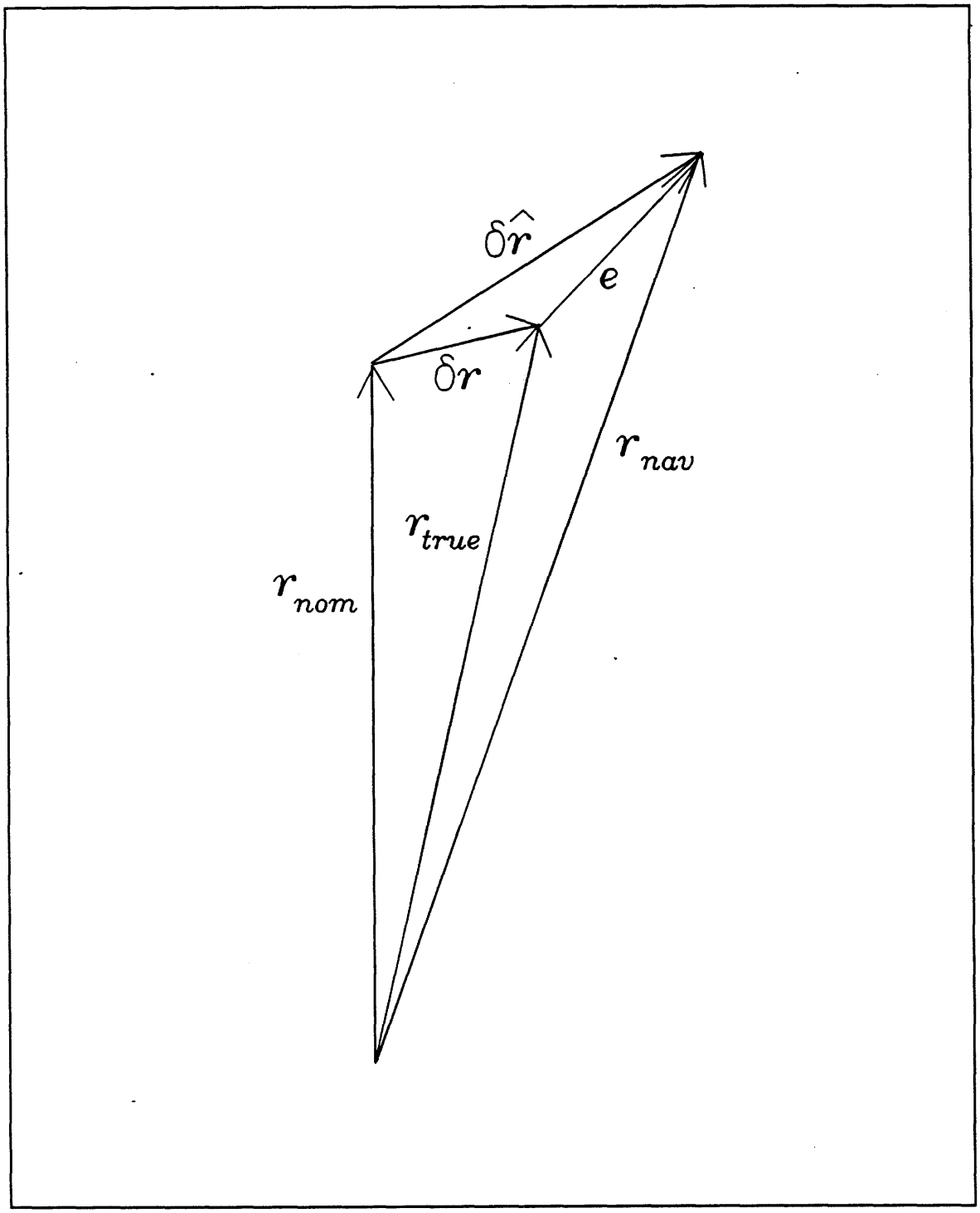

Figure 2.1 Perturbed Position Vectors

the error, and $\delta\hat{x}$ is the estimated dispersion from nominal. Figure 2.1 illustrates the relationship for the position vector. Notice that dispersions affect both the navigation and true state, while errors affect only the navigation state. Because errors and dispersions are small perturbations about the nominal, they are both propagated with the same time transition matrix, Φ_T.

A time slip, or initial time error, is converted to a dispersion, as developed in Section 2.2.1. A navigation time error is conceivable, though; in ref. [1], Battin develops a procedure for tracking clock inaccuracies by including time in the state. Also, if a spacecraft's clock differed from the ground, the time tag associated with a ground update would introduce further navigation errors. However, the accuracy of today's clocks makes these errors small enough to ignore. This study will assume perfect clocks and, therefore, end up with a 26 dimensional perturbation state: state errors, state dispersions, and time for each of the chaser and target vehicles. Table 2.1 summarizes the elements of the perturbation state.

In constructing the final augmented system, it is important to remember that the time slip affects dispersions only, and not errors (at least, to first order). Therefore, the dynamical state components associated with the navigation error in the augmented dynamical state and time transition matrix are zero. Equation (2.9), on page 33, shows the final linearized model of conic motion for propagating the errors and dispersions of two space craft to a nominal final time plus an equal time slip for both craft. The linearized, variable time of flight model of conic motion, developed here, will be the starting point for the calculation of the condition transition matrix in Section 2.3.

Table 2.1 Twenty-Six Dimensional Perturbation State Definition

Perturbation Type	Symbol		Description
Navigation Errors	e_c	δr_c	Chaser position (three components)
		δv_c	Chaser velocity (three components)
	e_t	δr_t	Target position (three components)
		δv_t	Target velocity (three components)
Dispersions	δx_c	δr_c	Chaser position (three components)
		δv_c	Chaser velocity (three components)
	δx_t	δr_t	Target position (three components)
		δv_t	Target velocity (three components)
	δt_c		Chaser time
	δt_t		Target time

$$e_{c_f} = \Phi_{T_c} e_{c_i}$$

$$e_{t_f} = \Phi_{T_t} e_{t_i}$$

$$\delta x_{c_f} = \Phi_{T_c} \delta x_{c_i} - \dot{x}_{c_f} \delta t_{c_i} + \dot{x}_{c_f} \delta t_s \quad \Rightarrow$$

$$\delta x_{t_f} = \Phi_{T_t} \delta x_{t_i} - \dot{x}_{t_f} \delta t_{t_i} + \dot{x}_{t_f} \delta t_s$$

$$\delta t_{c_f} = \delta t_{t_f} = \delta t_s$$

$$\delta x_A = \begin{bmatrix} e_c \\ e_t \\ \delta \dot{x}_c \\ \delta x_t \\ \delta t_c \\ \delta t_t \end{bmatrix} \qquad \dot{x}_A = \begin{bmatrix} \mathbf{0}_6 \\ \mathbf{0}_6 \\ \dot{x}_c \\ \dot{x}_t \\ 1 \\ 1 \end{bmatrix} \tag{2.9}$$

$$\Phi_A = \begin{bmatrix} \Phi_{T_c} & & & & & \\ & \Phi_{T_t} & & & & \\ & & \Phi_{T_c} & & -\dot{x}_{c_f} & \\ & & & \Phi_{T_t} & & -\dot{x}_{t_f} \\ & & & & 0 & \\ & & & & & 0 \end{bmatrix}$$

$$\delta x_{A_f} = \Phi_A \delta x_{A_i} + \dot{x}_{A_f} \delta t_s$$

2.3 The Condition Transition Matrix

As stated previously, the condition transition matrix differs from the time transition matrix in that the time of flight is not held constant. Instead, the flight time is allowed to vary so that a scalar termination condition can be maintained in the presence of perturbations. The methodology developed in this section is completely general and can be used to calculate a transition matrix for any scalar termination condition which can be defined by the state. This study focuses on a line of sight elevation angle which can be used to trigger an initial rendezvous burn.

Also discussed previously, the major simplification which allows this development is an assumption of linear motion at the terminal point. Because the actual motion is not linear, we are limited to 'small' time slips. The Monte Carlo simulation, developed in Chapter 3, will not only validate the analytic development, but also determine the region of linearity, giving us a feel for what is 'small'.

2.3.1 Varying Time of Flight to meet a Scalar Condition

Any arbitrary scalar maneuver condition, ξ, that can be defined by the terminal state, can be used to constrain a transition matrix by requiring the total derivative of the condition to be zero.

$$\delta\xi = \frac{\partial\xi}{\partial x_f}\delta x_f = \boldsymbol{k}^T\delta x_f = 0 \qquad (2.10)$$

where $\boldsymbol{k}^T$, the sensitivity, or constraint, vector, is the derivative of the desired

condition with respect to the terminal state. It should be mentioned that Tempelman allows for the possibility of a constraint condition involving both initial and final state perturbations. These are his, so called, traverse conditions, and, as a result, his equations are slightly more complicated. Traverse constraints can be defined for single vehicle motion, but with two vehicle motion, as in the case of rendezvous, they appear to have little meaning. For this reason, this study is restricted to terminal constraint conditions, that is, constraints that are functions of the terminal state only.

The final state is constrained by combining the linearized, variable time of flight model of conic motion (from equation (2.4)),

$$\delta x_f = \Phi_T \delta x_i + \dot{x}_f \delta t_s \tag{2.11}$$

with equation (2.10), which relates the desired constraint to the required change in flight time:

$$\delta \xi = k^T \delta x_f = k^T \Phi_T \delta x_i + k^T \dot{x}_f \delta t_s = 0 \tag{2.12}$$

Notice, from equation (2.12), the magnitude of k^T is not important, only its direction.

Equation (2.12) can now be solved for this time slip,

$$\delta t_s = \frac{-k^T \Phi_T \delta x_i}{k^T \dot{x}_f} \tag{2.13}$$

and inserted into equation (2.11):

$$\delta x_C = \Phi_T \delta x_i - \frac{\dot{x}_f k^T}{\dot{x}_f^T k} \Phi_T \delta x_i$$

$$= \left[I - \frac{\dot{x}_f k^T}{\dot{x}_f^T k} \right] \Phi_T \delta x_i \qquad (2.14)$$

$$= \Phi_I \Phi_T \delta x_i$$

$$= \Phi_C \delta x_i$$

which represents the constrained, linearized model of conic motion which terminates on the desired condition. It is completely general for any state that fully defines the desired terminal condition.

Using the augmented model developed in the previous section yields a desired advantage. Because the time error is included in the augmented state, and, from equation (2.9), $\delta t_s = \delta t_f$, equation (2.13) has not been lost. It has become a part of equation (2.14).

Equation (2.14) shows that the condition transition matrix is related to the time transition matrix by the dynamical state and the sensitivity vector.

$$\Phi_C = \left[I - \frac{\dot{x}_f k^T}{\dot{x}_f^T k} \right] \Phi_T \qquad (2.15)$$

$$= \Phi_I \Phi_T$$

Thus, the condition transition matrix is seen to be the product of two matrices: an idempotent matrix, Φ_I (an idempotent matrix is any matrix A, such that $A^2=A$), and the time transition matrix [10].

The result in equation (2.14) can be rewritten to show that the final constrained perturbation is the product of the idempotent matrix and final perturbation at the nominal terminal time.

$$\begin{aligned} \delta x_C &= \Phi_I \Phi_T \delta x_i \\ &= \Phi_I \delta x_f \end{aligned} \tag{2.16}$$

Because this matrix is idempotent, it can be interpreted as a 'shaping' matrix, shaping the perturbations to allow the final state to conform to the required condition. The idempotent property confirms that once a vector is shaped, any attempt to shape it again with the same matrix will have no effect; it is already constrained to the proper condition.

Combining equation (2.15) with equation (2.2) and then equation (2.1), yields the desired propagation of the covariance matrix to a condition and shows how the idempotent matrix 'shapes' a covariance matrix which has been propagated to a nominal final time.

$$\begin{aligned} E_C &= \Phi_C E_i \Phi_C^T \\ &= \Phi_I \Phi_T E_i \Phi_T^T \Phi_I^T \\ &= \Phi_I E_f \Phi_I^T \end{aligned} \tag{2.17}$$

2.3.2 Maneuver Conditions and the Sensitivity Vector

While the methodology developed is completely general and can be used to calculate a transition matrix for any terminal maneuver condition, this study focuses

on the elevation angle of the line of sight from the chaser craft to the target craft. This elevation angle is an observable condition which might be used to trigger a rendezvous burn. Four definitions for the elevation angle are developed. The first is the elevation of the line of sight with respect to the local horizontal of the chaser craft, and the second is the same angle with a correction if the target and chaser are not co-planer. The last two elevation angles are defined relative to the chaser's velocity vector. Figure 2.2 illustrates the elevation angles with no out of plane correction.

When the elevation angle is defined with respect to the local horizontal of the chaser craft, ϕ_1, it can be written as a function of the position vectors of the two spacecraft,

$$\sin\phi_1 = \frac{\Delta r^{\mathrm{T}} r_c}{|\Delta r||r_c|} \tag{2.18}$$

where $\Delta r = r_t - r_c$ is the relative position vector. The correction made in ϕ_2 removes the out of plane component of the relative position vector, essentially projecting the target's position onto the orbital plane of the chaser craft.

$$\begin{aligned}\sin\phi_2 &= \frac{\left[\Delta r - \frac{1}{h_c^2}\left(r_t^{\mathrm{T}} h_c\right) h_c\right]^{\mathrm{T}} r_c}{|\Delta r - \frac{1}{h_c^2}(r_t^{\mathrm{T}} h_c) h_c||r_c|} \\ &= \frac{\Delta r^{\mathrm{T}} r_c}{|\Delta r - \frac{1}{h_c^2}(r_t^{\mathrm{T}} h_c) h_c||r_c|}\end{aligned} \tag{2.19}$$

where $h = r \times v$ is the orbital angular momentum vector. ϕ_2 is also, therefore, a function of the chaser's velocity vector unless the two craft are co-planar, in which

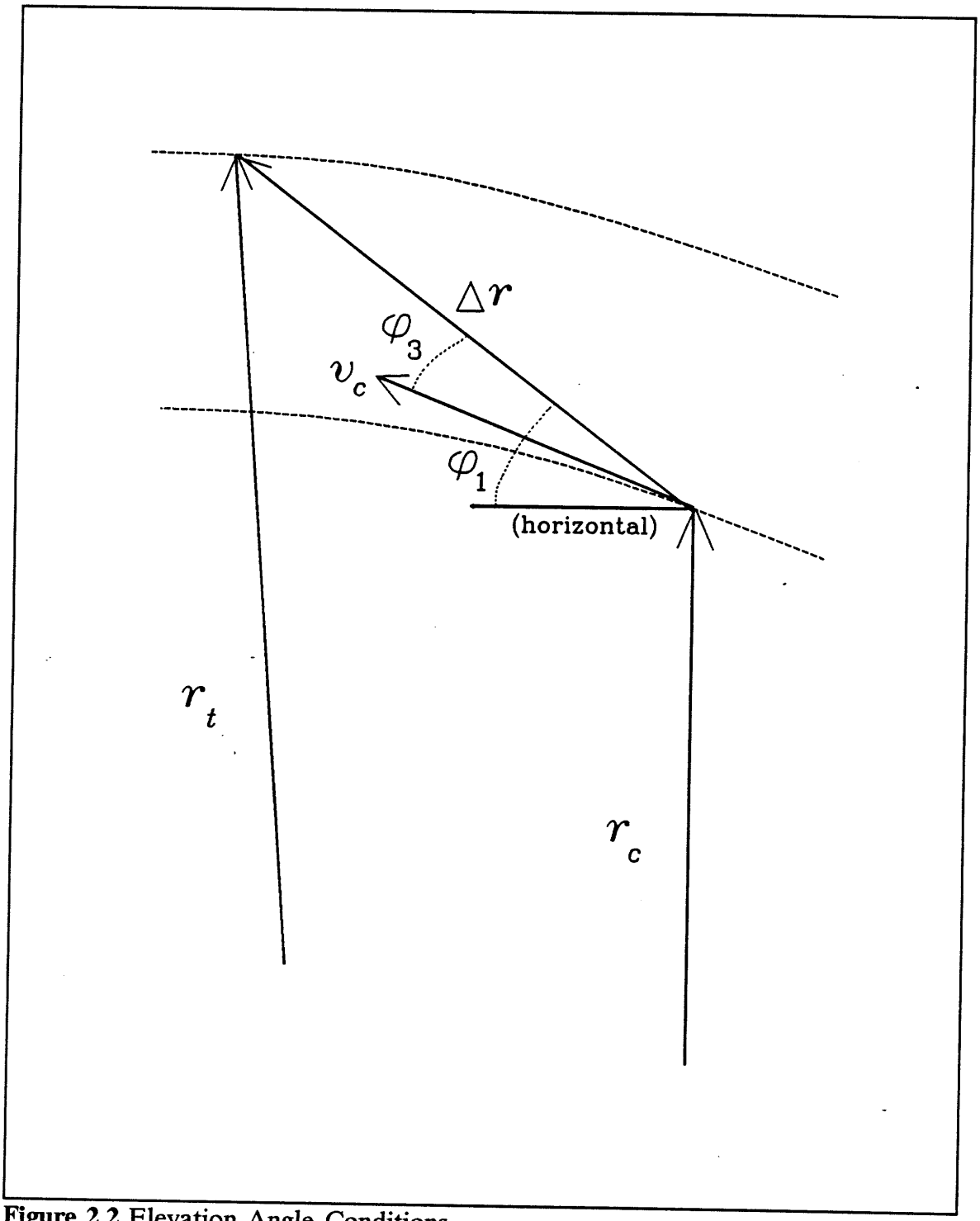

Figure 2.2 Elevation Angle Conditions

case equation (2.19) simplifies to equation (2.18).

ϕ_3 and ϕ_4 are defined similarly, but with respect to the chaser's velocity vector:

$$\cos\phi_3 = \frac{\Delta r^{\mathrm{T}} v_c}{|\Delta r||v_c|} \tag{2.20}$$

and

$$\begin{aligned}\sin\phi_4 &= \frac{\left[\Delta r - \frac{1}{h_c^2}\left(r_t^{\mathrm{T}} h_c\right) h_c\right]^{\mathrm{T}} v_c}{|\Delta r - \frac{1}{h_c^2}(r_t^{\mathrm{T}} h_c) h_c||v_c|} \\ &= \frac{\Delta r^{\mathrm{T}} v_c}{|\Delta r - \frac{1}{h_c^2}(r_t^{\mathrm{T}} h_c) h_c||v_c|}\end{aligned} \tag{2.21}$$

The sensitivity vector, which is the derivative of the desired condition with respect to the final state, is a row vector containing the partial derivatives of the condition with respect to each member of the state:

$$\begin{aligned}k_A^{\mathrm{T}} &= \frac{\partial\phi}{\partial x_{A_f}} \\ &= \left[\frac{\partial\phi}{\partial e_c}, \frac{\partial\phi}{\partial e_t}, \frac{\partial\phi}{\partial x_c}, \frac{\partial\phi}{\partial x_t}, \frac{\partial\phi}{\partial t_c}, \frac{\partial\phi}{\partial t_t}\right]\end{aligned} \tag{2.22}$$

where

$$\frac{\partial\phi}{\partial e} = \frac{\partial\phi}{\partial x} = \left[\frac{\partial\phi}{\partial r}, \frac{\partial\phi}{\partial v}\right] \tag{2.23}$$

Any members of the state which are not a direct function of the condition have a

zero partial derivative:

$$\frac{\partial \phi}{\partial t_c} = \frac{\partial \phi}{\partial t_t} = 0 \qquad \frac{\partial \phi}{\partial v_t} = \mathbf{0}_3^T \tag{2.24}$$

for all elevation angles defined.

Deriving the remaining partials for each elevation angle is a straight-forward, but messy exercise in differentiation. A few important steps and the results of the differentiation are contained in Appendix A. Note the magnitude of the sensitivity vector is not needed in calculating the condition transition matrix, so any scalar values common to all partials can be neglected, if desired.

CHAPTER 3
SIMULATION

A Monte Carlo simulation was written to validate the analytic development of Chapter 2 and to gain some knowledge of the size of perturbations that can be introduced without exceeding the region of linearity at the terminal point. This chapter describes the implementation of this simulation. Section 3.1 gives an overview of the main components of the simulation and describes two 'off the shelf' procedures used. Section 3.2 shows how representative error vectors were generated from a covariance matrix, detailing the statistical theory involved. The central procedure that propagated all the perturbed states to the condition and calculated the statistics is the subject of Section 3.3, and finally, the implementation of the analytic solution is discussed in Section 3.4.

3.1 Simulation Overview

The Monte Carlo simulation has six main components, as detailed in Table 3.1 (Their hierarchy is shown in Figure 3.1). Simulation Setup, the initializer and main executive, and two 'off the shelf' procedures, Telev and Kepler, are addressed in this section. The remaining components; the error generator, Monte

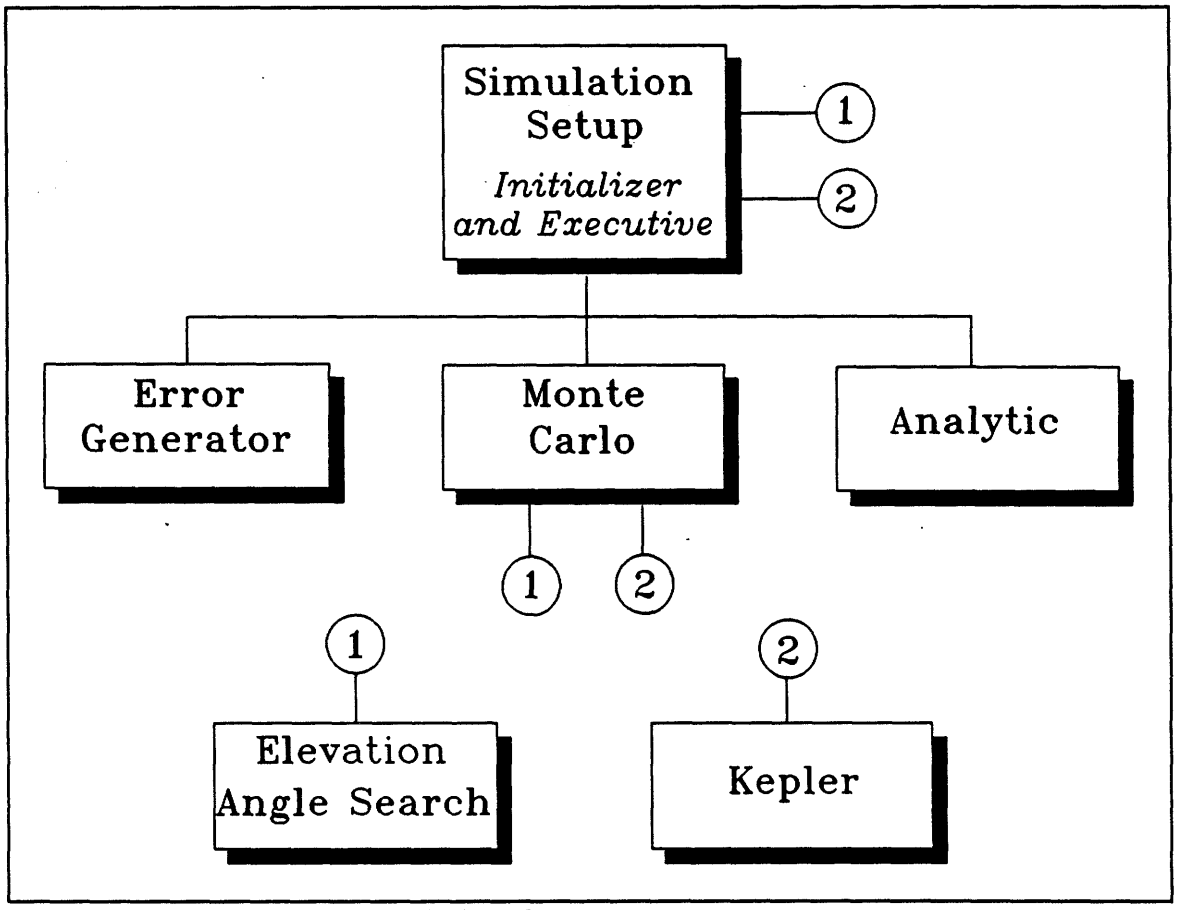

Figure 3.1 Hierarchy of Simulation Components

Table 3.1 Major Components of Computer Simulation

Program Component	Purpose
Simulation Setup	Initializes simulation and acts as main executive.
Elevation Angle Search	Finds the time a desired elevation angle condition will occur.
Kepler	Propagates a spacecraft's state to a new time and computes the time transition matrix.
Error Generator	Generates a statistically representative set of error vectors from an initial covariance matrix.
Monte Carlo	Propagates the perturbed states to the condition and calculates the statistics.
Analytic	Implements the analytic results of Chapter 2.

Carlo, and Analytic; are the subject of the following sections.

Inputs to the simulation are:

- Initial nominal state of the chaser in inertial frame.
- Initial nominal state of the target in inertial frame.
- Initial nominal time.
- Desired elevation angle.
- First guess for nominal time to achieve elevation angle condition.
- Type of elevation angle (from the four definitions).
- Initial augmented covariance matrix containing error and dispersion covariance data for the chaser and target.
- Covariance matrix scale factor.

Outputs are:

- Final twenty-six dimensional inertial covariance matrix propagated to

the desired condition by the **Monte Carlo** routine.

- Final twenty-six dimensional inertial covariance matrix propagated to the desired condition by the **Analytic** routine.
- Three dimensional Monte Carlo **estimated position dispersion** covariance matrix rotated to a relative line of sight frame.
- Three dimensional Analytic **estimated position dispersion** covariance matrix rotated to a relative line of sight frame.
- Three dimensional Monte Carlo **true position dispersion** covariance matrix rotated to a relative line of sight frame.
- Three dimensional Analytic **true position dispersion** covariance matrix rotated to a relative line of sight frame.

One sigma errors are also calculated from the main diagonals of each matrix.

Simulation Setup initializes the simulation by solving the nominal rendezvous problem. It calls Telev to find the nominal final time for the desired elevation angle condition, and Kepler to propagate the chaser and target states to this nominal condition (see Figure 3.2). It then acts as the executor, calling the error generator to obtain the initial augmented error set and then Monte Carlo and Analytic to generate the final condition covariance matrices.

$$x_{nom_i} \xrightarrow[\text{Telev, Kepler}]{\text{to condition}} x_{nom_c} ; \; t_{nom_c}$$

Figure 3.2 Propagating the Nominal State to an Elevation Angle Condition

Kepler is an 'off the shelf' procedure written by Stan Shepperd which propagates a position and velocity vector and computes a six dimensional time

transition matrix for a given time of flight. The procedure solves Kepler's problem and calculates the transition matrix using Goodyear's universal variables. Further information on the Kepler procedure can be found in ref. [7].

The elevation angle search component is also an 'off the shelf' procedure called Telev and taken from the space shuttle's on orbit software. It uses an iterative routine to find the time a desired elevation angle condition will occur and has been adapted to use the elevation angles defined in eqs. (2.18) through (2.21). It was set to use two body orbital mechanics. Further information on Telev can be found in ref. [5].

3.2 Error Generator

A procedure was written to generate any number of error vectors which accurately represent a given twenty-four dimensional covariance matrix (Initial time errors were assumed to be zero, with both craft starting on the same clock). The error generator takes advantage of the 'square root' covariance matrix devised by Jim Potter, as cited by Battin [1].

The development takes three steps [2]:

- A vector, y, of independent, gaussian random numbers with unit variance has covariance,

$$E[yy^T] = \overline{yy^T} = I \tag{3.1}$$

  where I is the identity matrix.

- The $n \times n$ symmetric, positive semidefinite covariance matrix, P,

representing the expected value of the outer product of an n dimensional error vector, e, with itself,

$$P = E[ee^T] = \overline{ee^T} \tag{3.2}$$

can be written as the product of a matrix, W, and its transpose:

$$P = WW^T \tag{3.3}$$

W is, therefore, a square root of P.

- A vector,

$$x = Wy \tag{3.4}$$

will have covariance,

$$E[xx^T] = W(E[yy^T])W^T = WW^T = P \tag{3.5}$$

The square root matrix, W, is not unique. One method of finding a square root matrix is to use the eigenvectors and eigenvalues:

$$P = V\Lambda V^T = V\Lambda^{\frac{1}{2}}\Lambda^{\frac{1}{2}}V^T = WW^T \tag{3.6}$$

where V is the matrix of unit eigenvectors (also called the modal matrix) and Λ is the diagonal eigenvalue matrix.

One commonly used error generating method takes advantage of this fact by interpreting the eigenvectors as 'directions' in n-space along which the components of the error vectors are uncorrelated. The eigenvalues are the variances of these components. The desired error vectors are then generated using the following equation:

$$x = \sum_{i=1}^{n} r_i \sqrt{\lambda_i} v_i \tag{3.7}$$

where r is an independent, gaussian random number with unit variance, and λ_i and v_i are the i^{th} eigenvalue and eigenvector of P [4]. Equation (3.7) can be seen to be equivalent to:

$$x = V\Lambda^{\frac{1}{2}} y = Wy \tag{3.8}$$

Calculating the eigenvectors and eigenvalues of a twenty-four dimensional matrix is a time consuming process, though. Fortunately, its also avoidable.

Because any square root matrix will do the trick, a much easier method assumes a lower triangular form for W [1]. This assumption allows the desired square root matrix to be determined by the straightforward solution of a series of simultaneous algebraic equations. While there are a variety of ways of doing this, the following easily programmed, recursive algorithm for an $n \times n$ positive semidefinite matrix, P, was borrowed from Cholesky and Banachiewicz, as cited in ref. [1]:

For $i=1, 2, ..., n$, the elements of W are calculated from

$$w_{ii} = \sqrt{p_{ii} - \sum_{j=1}^{i-1} w_{ij}^2}$$

$$w_{ji} = \begin{cases} 0 & \text{for } j<1 \\ \frac{1}{w_{ii}}\left(p_{ji} - \sum_{k=1}^{i-1} w_{jk} w_{ik}\right) & \text{for } j = i+1, i+2, \ldots, n \end{cases} \tag{3.9}$$

where w and p are the elements of W and P.

Because of the efficiency of this technique, it was also used to improve the computer's gaussian pseudo-random number generator when generating 'small' vector sets. After generating a set of independent, pseudo-random vectors, z, their covariance was calculated to be close to I, but not exact (the diagonal elements ranged from 0.92 to 1.07, and the off diagonal elements were as large as 0.08 for 1,001 twenty-four dimensional vectors). The computed covariance,

$$E[zz^T] = \overline{zz^T} = B = UU^T \approx I \tag{3.10}$$

where B is the near-identity covariance matrix, and U is its square root, was, therefore, 'divided' out to produce a set of vectors that really had independent elements with unit variance:

$$\begin{aligned} y &= U^{-1}z \\ E[yy^T] &= U^{-1}(E[zz^T])U^{-T} = U^{-1}BU^{-T} = I \end{aligned} \tag{3.11}$$

The new random vectors, y, indeed, had a covariance equal to the identity (to at least 15 figures). And the computed covariance of the resulting error vector set, $x = Wy$, matched the desired covariance, P, just as well. This 'fix' was derived independently, but was later found to be previously developed by Suddath in ref. [8].

3.3 Monte Carlo

The Monte Carlo component was written to solve the rendezvous problem for many randomly perturbed states obtained from the initial augmented covariance matrix. The Monte Carlo component propagates the generated error vectors to the

final condition, then re-calculates the statistics, forming the final condition covariance matrix.

For each augmented error vector, Monte Carlo builds an initial, true and navigation state from the initial nominal state, as defined in Chapter 2, for the chaser and the target:

$$x_{true_i} = x_{nom_i} + \delta x_i$$
$$x_{nav_i} = x_{true_i} + e_i \tag{3.12}$$

For each navigation state, it calls Telev to find the perturbed time for the desired elevation angle condition, and Kepler to propagate the estimated chaser and target states to this perturbed condition. It then calls Kepler again to propagate the true chaser and target states to the same perturbed time (see Figure 3.3).

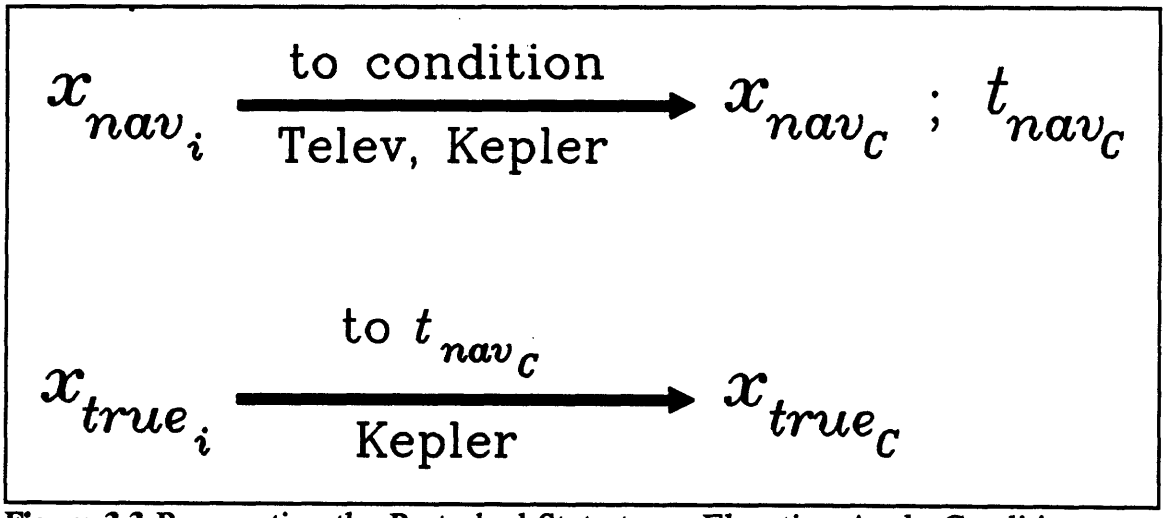

Figure 3.3 Propagating the Perturbed State to an Elevation Angle Condition

The final chaser and target condition perturbations are then calculated from these states by re-writing equation (3.12):

$$
\begin{aligned}
\delta t_C &= t_{nom_C} - t_{nav_C} \\
\delta \hat{x}_C &= x_{nav_C} - x_{nom_C} \\
\delta x_C &= x_{true_C} - x_{nom_C} \\
e_C &= \delta \hat{x}_C - \delta x_C
\end{aligned}
\tag{3.13}
$$

where the subscript, *C*, designates a state or perturbation propagated to the desired elevation angle condition.

Finally, an augmented final condition perturbation vector, δx_{A_C}, is built as defined in Table 2.1. These augmented vectors are then used to calculate the final condition covariance matrix:

$$
E_{A_C} = \overline{\delta x_{A_C} \delta x_{A_C}^T} \tag{3.14}
$$

3.4 Analytic Method

If the previous section seemed complex, it should serve to evoke an appreciation for an analytic method of propagating a covariance matrix to a maneuver condition. The simulation's Analytic component simply computed one (twenty-six dimensional) condition transition matrix using the equations developed in Chapter 2 and summarized here for clarity. As throughout this study, the six dimensional time transition matrix is assumed to be known, and was generated by Kepler.

The first, and, perhaps, most difficult, step is to calculate the augmented sensitivity vector, k_A^T:

$$k_A^T = \frac{\partial \phi}{\partial x_{A_f}} = \left[\frac{\partial \phi}{\partial e_{c_f}}, \frac{\partial \phi}{\partial e_{t_f}}, \frac{\partial \phi}{\partial x_{c_f}}, \frac{\partial \phi}{\partial x_{t_f}}, \frac{\partial \phi}{\partial t_c}, \frac{\partial \phi}{\partial t_t} \right] \tag{3.15}$$

where

$$\frac{\partial \phi}{\partial e} = \frac{\partial \phi}{\partial \dot{x}} = \left[\frac{\partial \phi}{\partial r}, \frac{\partial \phi}{\partial v} \right] \tag{3.16}$$

and

$$\frac{\partial \phi}{\partial t_c} = \frac{\partial \phi}{\partial t_t} = 0 \qquad \frac{\partial \phi}{\partial v_t} = 0_3^T \tag{3.17}$$

The remaining partials are located in Appendix A.

The augmented dynamical state and time transition matrix are then computed as follows:

$$\dot{x}_{A_f} = \begin{bmatrix} 0_6 \\ 0_6 \\ \dot{x}_{c_f} \\ \dot{x}_{t_f} \\ 1 \\ 1 \end{bmatrix} \qquad \text{where} \quad \dot{x} = \begin{bmatrix} v \\ a \end{bmatrix} \qquad \text{and} \quad a = \frac{-\mu r}{r^3} \tag{3.18}$$

$$\Phi_A = \begin{bmatrix} \Phi_{T_c} & & & & & \\ & \Phi_{T_t} & & & & \\ & & \Phi_{T_c} & & -\dot{x}_{c_f} & \\ & & & \Phi_{T_t} & & -\dot{x}_{t_f} \\ & & & & 0 & \\ & & & & & 0 \end{bmatrix} \tag{3.19}$$

which provides all the pieces necessary to compute the condition transition matrix:

$$\Phi_C = \left[I - \frac{\dot{x}_{A_f} k_A^T}{\dot{x}_{A_f}^T k_A} \right] \Phi_A \tag{3.20}$$

Individual augmented perturbation vectors were then propagated for comparison to Monte Carlo,

$$\delta x_C = \Phi_C \delta x_i \tag{3.21}$$

and the final condition covariance matrix was computed in one step:

$$E_C = \Phi_C E_i \Phi_C^T \tag{3.22}$$

The format for the output covariance matrices is presented in Chapter 4.

CHAPTER 4
RESULTS

Several test cases were used to validate the results of Chapter 2, investigate the region of linearity at the terminal point, and get a feel for the geometry of the perturbations at the desired condition. The results of these test cases are presented in this chapter.

The problem setup, including the initial covariance matrix and the nominal, initial and final vehicle states are presented in Section 4.1. Section 4.2 compares the final condition covariance matrices generated by the Monte Carlo and Analytic components of the simulation, verifying they agree. In Section 4.3, these matrices are transformed into a curvilinear coordinate frame to bring out the effect of the linearity assumption. Finally, in Section 4.4, an effort is made to visualize the perturbations at a maneuver condition by, first, using a different coordinate transformation to 'look' at the results in a relative, line of sight frame to see if the errors collapse along the line of sight, and then by comparing the estimated elevation angle error to the true elevation angle dispersion.

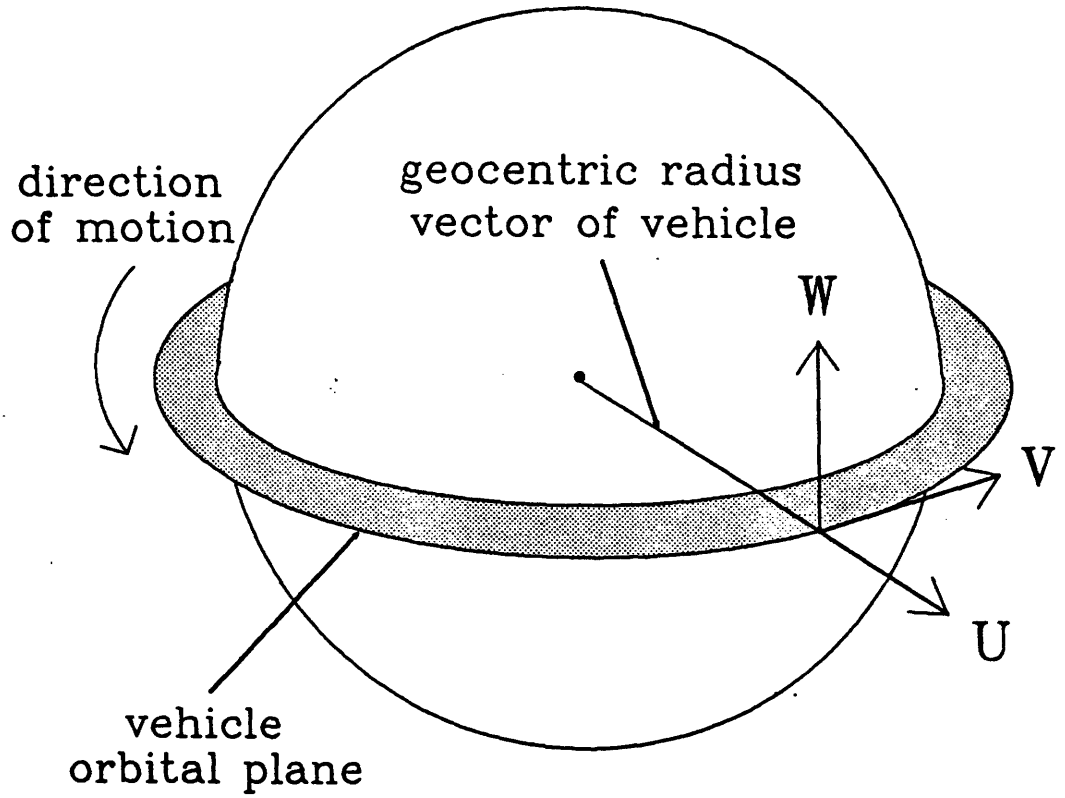

NAME: U, V, W coordinate system [5].

ORIGIN: Point of interest.

ORIENTATION: The U-V plane is the instantaneous orbit plane at epoch. The U axis lies along the geocentric radius vector to the vehicle and is positive radially outward.

The W axis lies along the instantaneous orbital angular momentum vector at epoch, and is positive in the direction of the angular momentum vector.

The V axis completes the right-handed orthogonal system.

CHARACTERISTICS: Quasi-inertial, right-handed, Cartesian coordinate system. This system is quasi-inertial in the sense that it is treated as an inertial coordinate system, but it is redefined at each point of interest.

Figure 4.1 UVW Coordinate System

4.1 Problem Setup

All test cases used the same initial covariance matrix. This covariance matrix reflects the uncertainty that exists in the ground uplink of a shuttle and target state during a shuttle rendezvous mission. The full six by six chaser and target covariance matrices, listed in Table 4.1, are expressed in the UVW coordinate frame (see Figure 4.1), and were rotated to the inertial frame for the initialization of each test case. Four assumptions were made in forming the initial augmented covariance matrix:

- Uncertainty in the errors and dispersions of each craft are equal.
- Correlations between chaser and target craft are zero.
- Correlations between errors and dispersions are zero.
- Initial time errors are zero.

The augmented covariance matrix was then multiplied by a scale factor to analyze the effects of scaled perturbations on the results.

Two different rendezvous orbits were used. The first had the target craft in a 200 NM altitude circular, equatorial orbit with the chaser ten miles below in a co-circular, co-planar orbit. The nominal final condition point was planned to occur with the chaser craft on the positive, inertial X axis. The second case had the target in a 200 by 29400 mile elliptic, equatorial orbit (eccentricity = 0.8) with the chaser, again, ten miles below in a co-elliptic, co-planar orbit. Periapsis coincided with the positive, inertial X axis, and the nominal final condition point was planned to occur with the chaser craft on the positive Y axis (true anomaly = 90°). The initial nominal state, as input to the simulation, and the final nominal state, as propagated

Table 4.1 Initial Covariance Matrices in UVW Frame

Chaser's Error and Dispersion Covariance Matrix:

3.83193E+05	−5.60173E+04	1.34268E+03	4.66259E+02	−3.02118E+02	−7.65116E−01
−5.60173E+04	2.35247E+06	−4.99017E+03	−2.18982E+03	−4.19257E+01	9.47873E−01
1.34268E+03	−4.99017E+03	1.17616E+06	6.96687E+00	−2.15600E+00	−4.06157E+02
4.66259E+02	−2.18982E+03	6.96687E+00	2.57924E+00	−2.96924E−01	−1.98502E−03
−3.02118E+02	−4.19257E+01	−2.15600E+00	−2.96924E−01	2.47009E−01	1.22858E−03
−7.65116E−01	9.47873E−01	−4.06157E+02	−1.98502E−03	1.22858E−03	3.81924E−01

Target's Error and Dispersion Covariance Matrix:

1.35124E+04	−1.48492E+04	3.59579E+02	2.47387E+01	−1.55673E+01	7.76503E−02
−1.48492E+04	9.08787E+05	−1.47445E+04	−1.07590E+03	1.32557E+01	−5.09445E+00
3.59579E+02	−1.47445E+04	1.06319E+06	1.86755E+01	−2.08800E+00	5.60670E+02
2.47387E+01	−1.07590E+03	1.86755E+01	1.28142E+00	−2.35343E−02	6.04941E−03
−1.55673E+01	1.32557E+01	−2.08800E+00	−2.35343E−02	1.82250E−02	−9.91980E−04
7.76503E−02	−5.09445E+00	5.60670E+02	6.04941E−03	−9.91980E−04	4.46224E−01

to the requested elevation angle by Simulation Setup, are listed in Table 4.2. The format used in this table to print the fourteen dimensional state vector is as follows:[†]

$$[\ r_{c_x}\ \ r_{c_y}\ \ r_{c_z}\ \ v_{c_x}\ \ v_{c_y}\ \ v_{c_z}$$
$$r_{t_x}\ \ r_{t_y}\ \ r_{t_z}\ \ v_{t_x}\ \ v_{t_y}\ \ v_{t_z}$$
$$t_c\ \ t_t\ \ ]$$

The desired elevation angle for each case was varied according to the orbit and the elevation type requested, so the nominal final points for all elevation types would be the same.[‡] For the co-circular orbits, a desired angle of 25.08 degrees was used. For the co-elliptic orbits, when the elevation was measured relative to the chaser's local horizontal (elevation types 1 and 2), 51.82° was used; when the elevation was measured relative to the chaser's velocity vector (types 3 and 4), 13.15° was used.

4.2 Validating the Analytic Result

The analytic result of Chapter 2 was validated in three ways. The first way used a separate simulation which propagated small deterministic dispersions with a fourteen dimensional condition transition matrix (no navigation errors). The Kepler procedure was then used to propagate the initial perturbed state to the same final time determined by the analytic method. The final elevation angle of the perturbed

[†]The units of measure used for all results are: feet, feet per second, seconds, and degrees, as appropriate.

[‡]Reference to elevation type in the results is from the four elevation angle definitions of Section 2.3.2.

Table 4.2 Nominal Simulation States

Initial Nominal State for Co-Circular Case:					
−3.84059E+06	−2.17811E+07	0.00000	2.48447E+04	−4.38080E+03	0.00000
−3.56721E+06	−2.18891E+07	0.00000	2.48654E+04	−4.05225E+03	0.00000
−1.53011E+03	−1.53011E+03				
Final Nominal State for Co-Circular Case:					
2.21171E+07	2.95695E−08	0.00000	−4.72937E−11	2.52280E+04	0.00000
2.21774E+07	1.29025E+05	0.00000	−1.46569E+02	2.51930E+04	0.00000
0.00000	0.00000				
Initial Nominal State for Co-Elliptic Case:					
−1.83697E+08	−3.40423E+07	0.00000	3.42607E+03	−3.44055E+03	0.00000
−1.83700E+08	−3.43293E+07	0.00000	3.44948E+03	−3.43606E+03	0.00000
−2.31422E+04	−2.31422E+04				
Final Nominal State for Co-Elliptic Case:					
−1.93715E−07	3.98168E+07	0.00000	−1.88024E+04	1.50471E+04	0.00000
−2.17846E+05	4.00938E+07	0.00000	−1.87778E+04	1.49204E+04	0.00000
0.00000	0.00000				

states, as produced by the analytic method and Kepler, were compared to the desired elevation angle. The results of this comparison, for several simple dispersions, are presented in Table 4.3. The analytic method is, indeed, finding the correct time slip and is propagating the dispersions to the desired condition.

The remaining methods of validation used the simulation described in Chapter 3. The first of these was a direct comparison of the augmented condition covariance matrices produced by the Analytic and Monte Carlo components. In the interest of conciseness, only the 'one sigma' uncertainties (the square root of the main diagonals) are presented here. For comparison, the uncertainties of the initial covariance matrix for the co-circular case are shown in Table 4.4. The format used in all remaining tables to print the twenty-six one sigma uncertainties is as follows:

$$
\begin{bmatrix}
e_{c_x} & e_{c_y} & e_{c_z} & \dot{e}_{c_x} & \dot{e}_{c_y} & \dot{e}_{c_z} \\
e_{t_x} & e_{t_y} & e_{t_z} & \dot{e}_{t_x} & \dot{e}_{t_y} & \dot{e}_{t_z} \\
\delta r_{c_x} & \delta r_{c_y} & \delta r_{c_z} & \delta v_{c_x} & \delta v_{c_y} & \delta v_{c_z} \\
\delta r_{t_x} & \delta r_{t_y} & \delta r_{t_z} & \delta v_{t_x} & \delta v_{t_y} & \delta v_{t_z} \\
\delta t_c & \delta t_t &]
\end{bmatrix}
$$

The order is as defined in Table 2.1, with a position and velocity perturbation vector on each row.

Table 4.5 compares the results for a co-circular case in which the initial covariance matrix was scaled by a factor of one sixteenth. As hoped, both simulation components are producing, essentially, the same condition covariance matrices. Also noteworthy, is the relative sizes of the perturbations. The errors stayed about the same size as the initial errors, while the dispersions grew dramatically. This is due to the time slip. The average time slip (about 17 seconds,

Table 4.3 Elevation Angle Accuracy Using Analytic Method

Initial Error	δt_s (s)	Elevation Error (deg)	
		Analytic	Kepler
δr_x = 10 ft	0.193	-1.2E-6	-2.4E-7
δr_y = 10 ft	0.804	-2.0E-5	-8.9E-6
δv_x = 0.1 ft/s	4.573	-9.2E-4	-5.9E-4
δv_y = 0.1 ft/s	-4.602	-5.9E-4	-2.3E-4
δr_c = [1, -3, 0] δv_c = [-0.1, 0.3, 0] δr_t = [-1, 4, 0] δv_t = [-0.04, -0.09, 0] δt_c = 1E-8 δt_t = 0	-7.691	-2.3E-3	-1.4E-3

Table 4.4 Initial Covariance Matrix - Co-Circular, Covariance Scale Factor 1, Inertial Frame

One Sigma Uncertainties From Main Diagonal:

1.52061E+03	6.50703E+02	1.08451E+03	6.47216E−01	1.55157E+00	6.18000E−01
9.43578E+02	1.78773E+02	1.03111E+03	2.41615E−01	1.11412E+00	6.68000E−01
1.52061E+03	6.50703E+02	1.08451E+03	6.47216E−01	1.55157E+00	6.18000E−01
9.43578E+02	1.78773E+02	1.03111E+03	2.41615E−01	1.11412E+00	6.68000E−01
0.00000	0.00000				

Table 4.5 Comparison of Final Condition Covariance Matrices - Co-Circular, Elevation Type 1, Covariance Scale Factor 0.0625, Inertial Frame

One Sigma Uncertainties From Main Diagonal:

ANALYTIC:

2.39691E+02	7.69378E+02	1.66196E+02	8.00467E−01	2.25876E−01	2.89095E−01
2.41656E+01	2.86411E+02	1.12794E+02	3.12385E−01	2.24063E−02	3.11802E−01
2.39691E+02	4.38899E+05	1.66196E+02	5.00695E+02	2.25876E−01	2.89095E−01
2.55629E+03	4.38855E+05	1.12794E+02	4.98525E+02	2.89725E+00	3.11802E−01
1.74177E+01	1.74177E+01				

MONTE CARLO:

2.41163E+02	7.69301E+02	1.66159E+02	8.00686E−01	2.25955E−01	2.89123E−01
2.47189E+01	2.86351E+02	1.12647E+02	3.12309E−01	2.33777E−02	3.11871E−01
7.31356E+03	4.36274E+05	1.66004E+02	4.97700E+02	8.37151E+00	2.89239E−01
7.95173E+03	4.36231E+05	1.12990E+02	4.95544E+02	9.03020E+00	3.11710E−01
1.73170E+01	1.73170E+01				

Table 4.6 Comparison of Final Condition Covariance Matrices - Co-Elliptic, Elevation Type 3, Covariance Scale Factor 0.01, Inertial Frame

One Sigma Uncertainties From Main Diagonal:

ANALYTIC:

4.91245E+03	4.28278E+03	5.92013E+02	3.65586E−01	2.28709E+00	2.82168E−01
3.65232E+03	3.15071E+03	6.72483E+02	1.49546E−01	1.68834E+00	3.00228E−01
1.13589E+06	9.09298E+05	5.92013E+02	3.65586E−01	5.36496E+02	2.82168E−01
1.13830E+06	9.04527E+05	6.72483E+02	2.91747E+00	5.30792E+02	3.00228E−01
6.05487E+01	6.05487E+01				

MONTE CARLO:

4.90978E+03	4.28722E+03	5.92390E+02	3.72361E−01	2.29196E+00	2.82249E−01
3.65080E+03	3.15846E+03	6.71716E+02	1.54584E−01	1.69562E+00	3.00885E−01
1.13306E+06	9.06152E+05	5.92372E+02	1.34829E+01	5.34592E+02	2.82243E−01
1.13548E+06	9.01415E+05	6.73257E+02	1.34324E+01	5.28922E+02	3.00131E−01
6.04241E+01	6.04241E+01				

in this case) shows itself in the dispersions, while the errors are unaffected, as stated in the development.

The co-elliptic case, presented in Table 4.6, validates the development using the elevation angle as measured from the chaser's velocity vector. Again, Analytic and Monte Carlo produce, essentially, the same results. In this case, the elevation type makes a significant difference. As shown, with elevation type 3, the average time slip is 60.5 seconds. When the same case, with the same covariance scale factor, was run with the elevation defined off the local horizontal (elevation type 1, not shown), the average time slip required was only 24.1 seconds (As mentioned in the previous section, the requested elevation angle was varied for each elevation type so the **nominal** final positions of both craft would be the same).

The final method of validation looked at the average elevation error. The sensitivity vector and the final condition transition matrix are used to calculate a scalar variation in the elevation angle:

$$\begin{aligned} \delta\phi &= \frac{\partial\phi}{\partial x_{A_C}}\delta x_{A_C} \\ &= k_A^T \delta x_{A_C} \end{aligned} \quad \Rightarrow \quad \begin{aligned} \overline{\delta\phi^2} &= k_A^T\left(\overline{\delta x_{A_C}\delta x_{A_C}^T}\right)k_A \\ &= k_A^T \Phi_C k_A \end{aligned} \tag{4.1}$$

Of course, this value is guaranteed to be (and is) zero using the analytic method, because

$$k_A^T \Phi_I = 0^T \tag{4.2}$$

but the fact it is near zero when using Monte Carlo's output validates both the sensitivity vector derivation and the Monte Carlo method. Table 4.7 summarizes the average elevation error (the square root of equation (4.1)) for several test cases.

Table 4.7 Estimated Average Elevation Angle Error Calculated From the Condition Covariance Matrix

Orbit	Elevation Type	Covariance Scale Factor	Average Elevation Error	
			Analytic	Monte Carlo
co-circular	1	25	2E-5	2.9
		4	7E-7	0.6
		1	2E-6	0.2
		6.25E-2	1E-6	1E-2
co-elliptic	1	1E-2	2E-7	1E-2
	3	1E-2	3E-6	4E-2

4.3 The Linearity Assumption

The assumption of linear motion at the terminal point cannot be taken for granted, because, obviously, it must break down somewhere. For 'small' enough perturbations in time, though, a linear region must exist. To bring out the effect of the linearity assumption, the individual twenty-six dimensional perturbation vectors, which were propagated to the condition by Monte Carlo and Analytic, were transformed to a local vertical, curvilinear (LVC) coordinate system (see Figure 4.2). These transformed vectors were then used to compute a new LVC condition covariance matrix. By separating the downrange (X_{lvc}) and altitude (Z_{lvc}) perturbations, a vehicle, which has been propagated linearly, can be seen 'gaining altitude' above the actual curved flight path. The linearity assumption is, therefore,

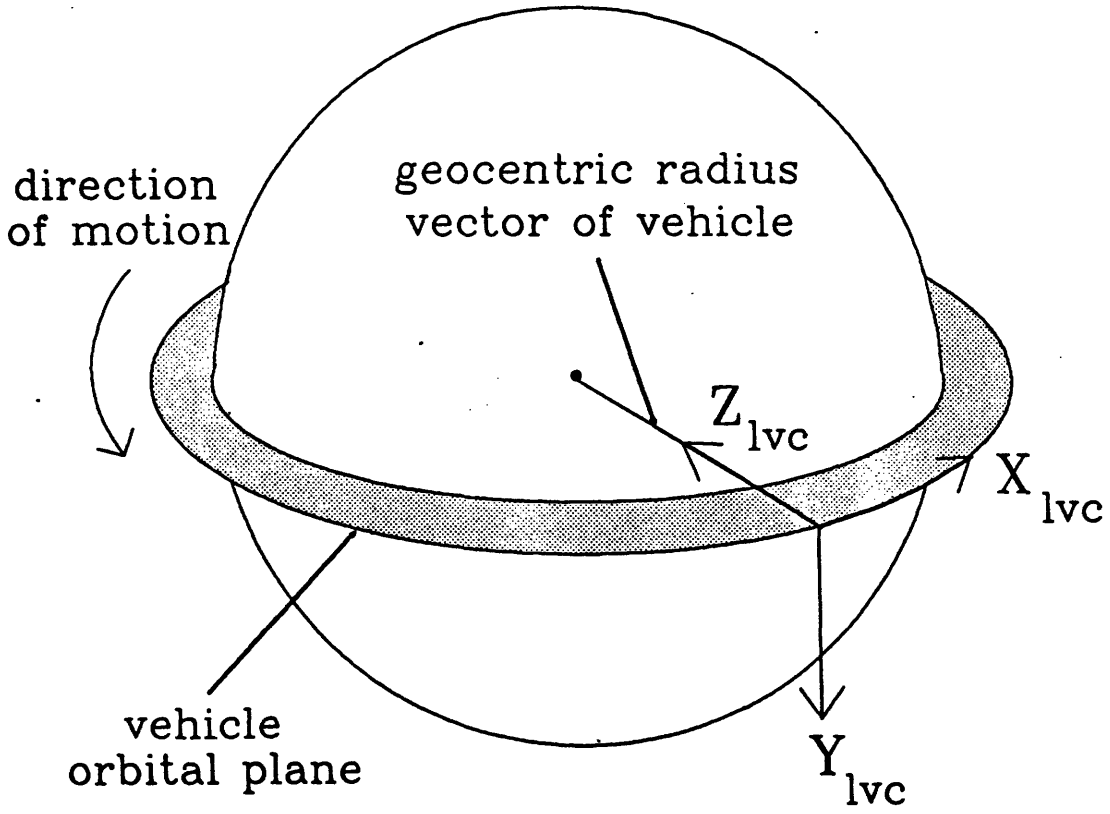

NAME: Local vertical, curvilinear coordinate system.

ORIGIN: Nominal vehicle center of mass.

ORIENTATION: The X_{lvc}-Z_{lvc} plane is the instantaneous orbit plane of the nominal trajectory. The Z_{lvc} axis lies along the geocentric radius vector to the vehicle and is positive toward the center of the earth, measuring radial distance from the nominal flight path.

The X_{lvc} axis curves along the vehicle's path of flight, perpendicular to the Z_{lvc} axis, and is positive in the direction of motion, measuring downrange distance along the flight path.

The Y_{lvc} axis is normal to the orbit plane and completes the right-handed orthogonal system.

CHARACTERISTICS: Right-handed, curvilinear, rotating coordinate system.

Figure 4.2 Nominal Vehicle-Centered, Local Vertical, Curvilinear Coordinate System

seen to introduce an altitude dispersion that is not really there. For small time slips, this added dispersion is also small, but for larger slips, the dispersion gets to be excessive.

The co-circular orbit case, with two different sized initial covariance matrices is presented to show this effect. In Table 4.8, the same case and covariance scale factor as for Table 4.5 are used. Note the altitude dispersions for the analytic component are larger than for Monte Carlo. For Monte Carlo, the full effect of the time slip is seen in the downrange dispersions. For Table 4.9, the covariance scale factor is increased to 1, and the effect is more pronounced. The altitude dispersion has grown to about one tenth the downrange dispersion in the analytic covariance matrix.

Next, with a good knowledge of the direct effect of the linearity assumption, it is necessary to measure the accuracy of the analytic component in keeping the elevation error small as the size of the initial perturbations are increased. A more direct measure of the actual estimated average elevation error was obtained by calculating the elevation angle of the final navigation states produced by the Analytic and Monte Carlo components from each initial perturbation vector and then calculating how this varied from the nominal. Table 4.10 presents this result for the same cases presented in Table 4.7. Note that when the elevation error is calculated by this method, Monte Carlo is very consistent (reflecting the elevation tolerance required of the iterative elevation angle search procedure), but Analytic starts to break down with very large perturbations. The effect of large perturbations on the ability of the sensitivity vector to calculate an accurate elevation angle variance can now be recognized in Table 4.7, too.

Another measure of the accuracy of the analytic method is its ability to find the correct time slip. Table 4.11 shows the one sigma time slips obtained by

Table 4.8 Comparison of Final Condition Covariance Matrices - Co-Circular, Elevation Type 1, Covariance Scale Factor 0.0625, LVC Frame

One Sigma Uncertainties From Main Diagonal:

ANALYTIC:

7.69021E+02	1.66196E+02	2.39948E+02	4.97599E−01	2.89095E−01	1.13777E−01
2.86382E+02	1.12794E+02	2.38315E+01	4.96460E−02	3.11802E−01	3.70283E−02
4.38733E+05	1.66196E+02	**7.38400E+03**	4.97534E−01	2.89095E−01	1.14011E−01
4.38699E+05	1.12794E+02	**7.34485E+03**	4.96366E−02	3.11802E−01	3.70405E−02
1.74177E+01	1.74177E+01				

MONTE CARLO:

7.69801E+02	1.66159E+02	2.39560E+02	4.97720E−01	2.89123E−01	1.12898E−01
2.86489E+02	1.12647E+02	2.30692E+01	4.96883E−02	3.11871E−01	3.70330E−02
4.36355E+05	1.66004E+02	**2.39518E+02**	4.97626E−01	2.89239E−01	1.12962E−01
4.36324E+05	1.12990E+02	**2.30616E+01**	4.96737E−02	3.11710E−01	3.70350E−02
1.73170E+01	1.73170E+01				

Table 4.9 Comparison of Final Condition Covariance Matrices - Co-Circular, Elevation Type 1, Covariance Scale Factor 1, LVC Frame

One Sigma Uncertainties From Main Diagonal:

ANALYTIC:

3.04724E+03	6.64784E+02	9.99848E+02	1.97034E+00	1.15638E+00	4.98496E−01
1.13879E+03	4.51177E+02	1.30122E+02	1.98017E−01	1.24721E+00	1.48148E−01
1.74521E+06	6.64784E+02	**1.17176E+05**	1.96838E+00	1.15638E+00	5.03737E−01
1.74514E+06	4.51177E+02	**1.16779E+05**	1.97890E−01	1.24721E+00	1.48286E−01
6.96710E+01	6.96710E+01				

MONTE CARLO:

3.08807E+03	6.66729E+02	9.54406E+02	1.98230E+00	1.15493E+00	4.57677E−01
1.14568E+03	4.53618E+02	9.27440E+01	1.99852E−01	1.24606E+00	1.47775E−01
1.75331E+06	6.64571E+02	**9.53523E+02**	1.98033E+00	1.15655E+00	4.59001E−01
1.75318E+06	4.59074E+02	**9.27005E+01**	1.99803E−01	1.24348E+00	1.47745E−01
6.95810E+01	6.95810E+01				

Table 4.10 Estimated Average Elevation Angle Error Calculated From the Error Vectors

Orbit	Elevation Type	Covariance Scale Factor	Average Elevation Error	
			Analytic	Monte Carlo
co-circular	1	25	2.7	4E-3
		4	0.6	4E-3
		1	0.2	3E-3
		6.25E-2	1E-2	4E-3
co-elliptic	1	1E-2	2E-2	5E-3
	3	1E-2	4E-2	3E-3

Table 4.11 Average Time Slip Comparison

Orbit	Elevation Type	Covariance Scale Factor	Average Time Slip		Average Time Slip Difference
			Analytic	Monte Carlo	
co-circular	1	25	348	335	13
		4	139.3	138.7	0.7
		1	69.7	69.6	0.1
		6.25E-2	17.4	17.3	0.1
co-elliptic	1	1E-2	24.1	24.3	-0.2
	3	1E-2	60.5	60.4	0.1

Analytic and Monte Carlo, and their difference. The average time slip obtained from Analytic starts to diverge from that of Monte Carlo as the perturbations grow. Both measures, the elevation angle error and the average time slip difference, give a feel for what 'small' perturbations are for these orbits.

Unfortunately, the definition of 'small' will change for each rendezvous scenario. Factors which affect how quickly altitude errors build up, and, thus, how large an acceptable time slip can be, are the curvature of the actual flight path and the speed of the vehicle. This means the size of the orbit and, for elliptic orbits, the vehicle's position in the orbit will affect the definition of small. Many factors will also affect how quickly the condition constraint is changing, and, therefore, the size of the time slip required. In the final analysis, though, the size of the time slips required is primarily a function of how well the problem is defined. It may well be the case that the analytic method developed here will not be applicable to certain ill-defined problems requiring large time slips which violate the region of linearity.

4.4 Visualizing Perturbations at a Maneuver Condition

Trying to think in twenty-six dimensions is a little difficult. This makes 'seeing' what the perturbations at a maneuver condition look like equally difficult. Any effort to reduce the dimensionality of the problem is a great help. The LVC frame was useful to show that the perturbations were really about the same size, but just spread up and down range from nominal. Another transformation to a relative, line of sight (LOS) coordinate system is also helpful (see Figure 4.3 for a definition). By going to a relative frame, which expresses the chaser's position relative to the target, the dimensionality is cut to twelve (there is no relative time difference

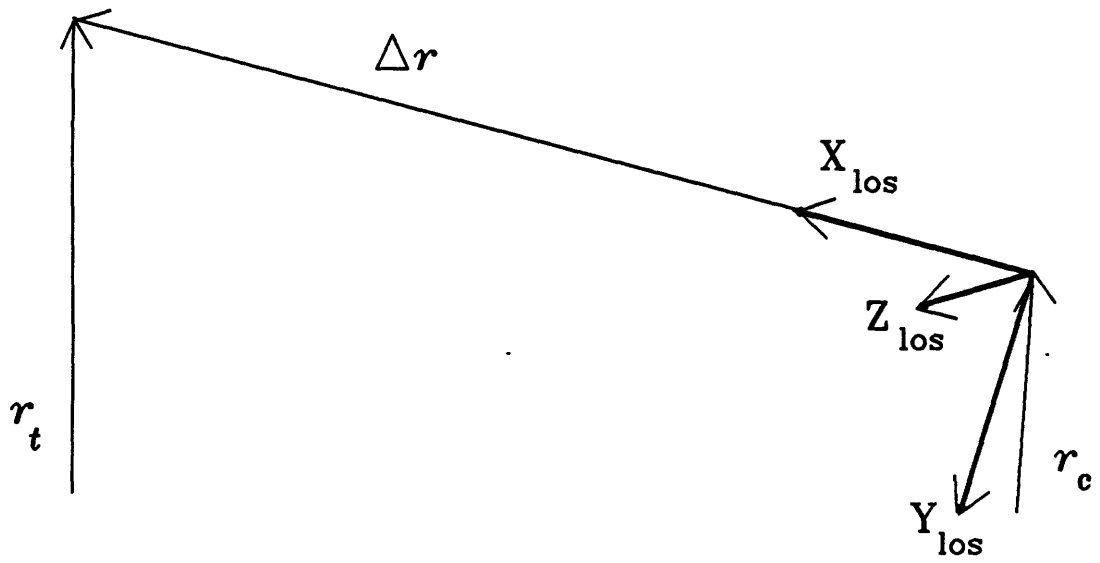

NAME: Line of sight coordinate system.

ORIGIN: Chaser vehicle center of mass.

ORIENTATION: The X_{los}-Y_{los} plane is the instantaneous plane spanned by the geocentric radius vectors of the chaser and target vehicles. The X_{los} axis lies along the relative position vector and is positive toward the target vehicle. This is the line of sight from the chaser to the target.

The Z_{los} axis is normal to the X_{los}-Y_{los} plane, and is positive-in the direction of a vector which is the vector cross product of the chaser and target geocentric radius vectors.

The Y_{lvc} axis is perpendicular to the relative position vector and completes the right-handed orthogonal system.

CHARACTERISTICS: Right-handed, Cartesian, rotating coordinate system. This system is designed so the elevation angle, as defined in equation (2.18), will lie in the X_{los}-Y_{los} plane. A slightly different line of sight frame is used with each elevation angle definition to keep the angle in this plane.

Figure 4.3 Line of Sight Coordinate System

between vehicles). Neglecting velocity errors and dispersions, we can then look at estimated **position** dispersions and true **position** dispersions separately, and the problem is down to three dimensions. The former shows how the navigation position estimate is dispersed from the nominal, and the latter shows the true position dispersions from the nominal.

Intuition would suggest that when the line of sight is held constant relative to the local horizontal or the velocity vector, that the error perpendicular to the line of sight and in the relative plane (Y_{los}) would be zero when the condition is achieved. The error vector is said to 'collapse' along the line of sight. This is impossible to see in an inertial frame, though, because the local horizontal and the velocity vector, and thus the LOS frame, are rotating with time. And because time is allowed to slip, the times associated with the nominal and perturbed states are different. Figure 4.4 illustrates how perturbing a state from the nominal with a time slip affects the LOS frame, and, therefore, shows that when time is allowed to slip, the LOS frame for the perturbed state must also be rotated to compensate.

An inertial, time varying perturbation vector or covariance matrix cannot, then, be simply rotated to the LOS frame. In fact, a different perturbation vector is needed. In an inertial frame,

$$\delta\Delta r = \Delta r_{pert} - \Delta r_{nom} \tag{4.3}$$

but to obtain a time varying, LOS perturbation vector, the LOS frame for the perturbed state must, first, be rotated to account for the time slip:

$$\delta\Delta r_{los} = A(\omega\,\delta t_f)\,\Delta r_{pert} - \Delta r_{nom} \tag{4.4}$$

where $A(\omega\delta t_f)$ is a rotation matrix,

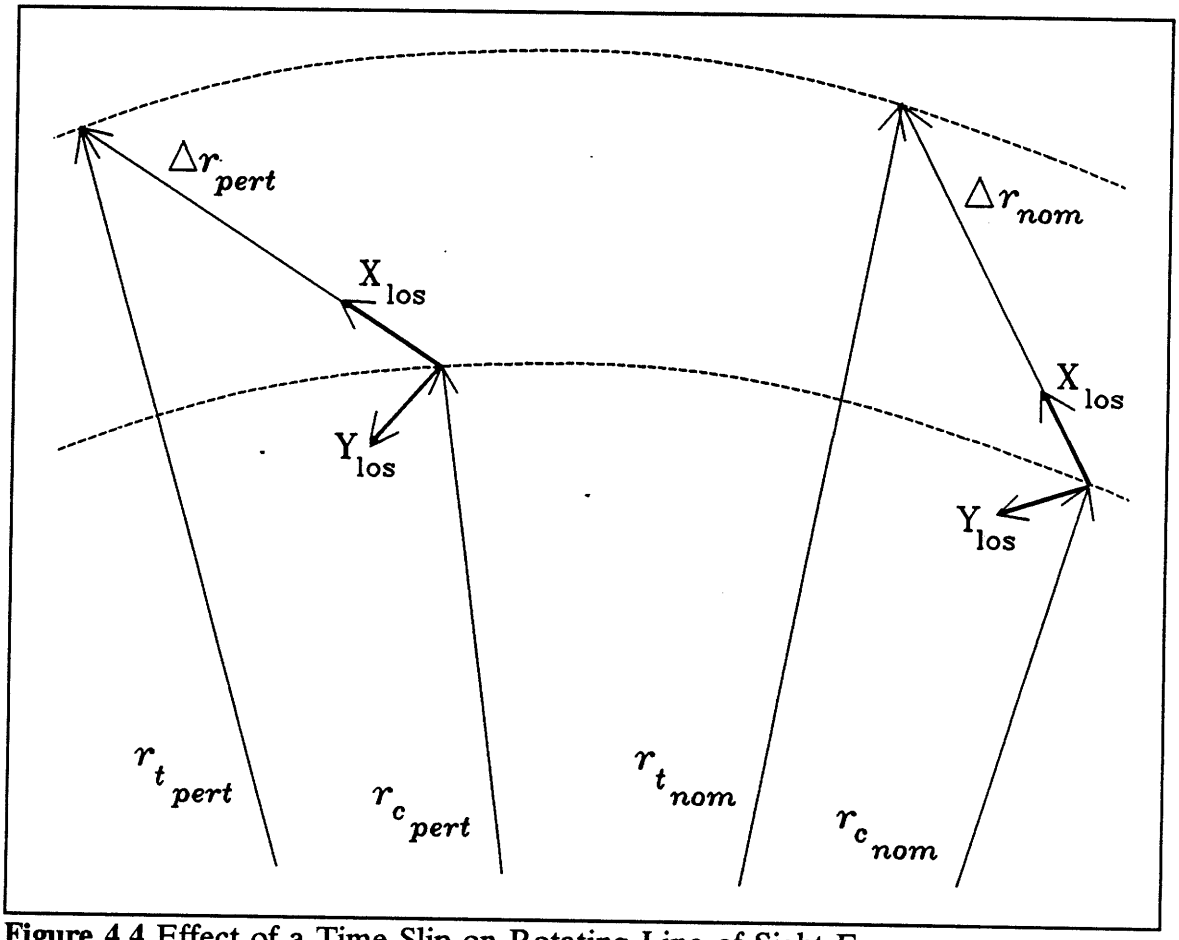

Figure 4.4 Effect of a Time Slip on Rotating Line of Sight Frame

$$A(\omega\,\delta t_f) = \begin{bmatrix} \cos(\omega\,\delta t_f) & \sin(\omega\,\delta t_f) & 0 \\ -\sin(\omega\,\delta t_f) & \cos(\omega\,\delta t_f) & 0 \\ 0 & 0 & 1 \end{bmatrix} \tag{4.5}$$

and ω is the angular velocity of the chaser orbit. This is the only rotation needed when the line of sight is held constant relative to the local horizontal. When it is held constant relative to the velocity vector, an additional rotation must be made to account for the angular rotation of the velocity vector with respect to the local horizontal. This is accomplished by substituting $(\omega + \dot{\gamma})$ for ω in equation (4.5), where $\dot{\gamma}$ is the time rate of change of the flight path angle:

$$\dot{\gamma} = \frac{d\gamma}{dt} = \frac{h(\mu - rv^2)}{r^3 v^2} \tag{4.6}$$

where μ is the gravitational parameter. These new LOS perturbation vectors, which were calculated using the twenty-six dimensional inertial perturbation vectors propagated to the condition by Analytic and Monte Carlo, were then used to compute a new LOS condition covariance matrix.

Often, in covariance analysis, the question is, what happens to the true state when maneuvers are made based on the navigation estimate of the state. In this case, the navigation state is constrained to a condition, but the true state is not. The transformation to the LOS coordinate system lets us see the effect. In Table 4.12, the co-circular orbits case with a 1/16 covariance scale factor is presented in the LOS frame. The estimated position dispersion and true position dispersion covariance matrices, as calculated from the inertial perturbation vectors produced by Analytic and Monte Carlo, are shown, as well as their associated one sigma uncertainties. As suggested by intuition, the estimated position dispersion

Table 4.12 Comparison of Final Condition Covariance Matrices - Co-Circular, Elevation Type 1, Covariance Scale Factor 0.0625, LOS Frame

RELATIVE ANALYTIC ESTIMATED POSITION DISPERSION COVARIANCE MATRIX:

6.261913020919E+05	5.347329338515E+03	−2.540297561973E+02
5.347329338515E+03	7.031911858011E+02	−6.229824767212E+01
−2.540297561973E+02	−6.229824767212E+01	8.068720629973E+04

One Sigma Uncertainties From Main Diagonal:

7.913225019497E+02	**2.651775227656E+01**	2.840549353553E+02

RELATIVE MONTE CARLO ESTIMATED POSITION DISPERSION COVARIANCE MATRIX:

6.138037833267E+05	1.444583188955E+03	3.459318429782E+02
1.444583188955E+03	8.276183539467E+01	−3.999286987816E+01
3.459318429782E+02	−3.999286987816E+01	8.062224383743E+04

One Sigma Uncertainties From Main Diagonal:

7.834563059461E+02	**9.097353208196E+00**	2.839405639169E+02

RELATIVE ANALYTIC TRUE POSITION DISPERSION COVARIANCE MATRIX:

1.644869483409E+06	6.355364742566E+05	−2.929294122991E+02
6.355364742566E+05	3.020465862788E+05	−2.364784855042E+02
−2.929294122991E+02	−2.364784855042E+02	4.034360314986E+04

One Sigma Uncertainties From Main Diagonal:

1.282524652164E+03	**5.495876511338E+02**	2.008571710193E+02

RELATIVE MONTE CARLO TRUE POSITION DISPERSION COVARIANCE MATRIX:

1.626745360030E+06	6.276790262117E+05	4.211591150865E+02
6.276790262117E+05	2.979182713376E+05	2.452058269794E+02
4.211591150865E+02	2.452058269794E+02	4.036887999681E+04

One Sigma Uncertainties From Main Diagonal:

1.275439281201E+03	**5.458188997622E+02**	2.009200836074E+02

(navigation's deviation from nominal) perpendicular to the line of sight and in the relative plane (Y_{los}) is very small for both Analytic and Monte Carlo, but the true position dispersion (true deviation from nominal), in the same direction, is not. Table 4.13 reveals the same effect for the co-elliptic case with a 0.01 covariance scale factor. It really is easier to 'see' what is happening with the problem reduced to three dimensions.

The effect on the true state caused by performing maneuvers based on the estimated state can also be seen by comparing the average elevation angle error calculated from the estimated state with the average elevation angle dispersion calculated from the true state. The true average elevation dispersion can be calculated in two ways, just as the estimated average error was. Table 4.7 showed the estimated average elevation error as calculated with the sensitivity vector and the condition covariance matrix using equation (4.1). The true average elevation dispersion can also be calculated using this equation by substituting a sensitivity vector which reflects only the sensitivity of the elevation angle to dispersions. This is accomplished by nulling the first twelve components of k_A^T. The resulting true average elevation dispersions are presented in Table 4.14.

The second method of calculating the true average elevation dispersion uses the variance from nominal of the true elevation angle as calculated from the final true states produced by the Analytic and Monte Carlo components. This is similar to the method used to find the estimated average elevation errors in Table 4.10. This second method is not subject to the linearity problems that the sensitivity vector encounters for large perturbations. The true average elevation errors calculated by this method are shown in Table 4.15.

Table 4.13 Comparison of Final Condition Covariance Matrices - Co-Elliptic, Elevation Type 3, Covariance Scale Factor 0.01, LOS Frame

RELATIVE ANALYTIC ESTIMATED POSITION DISPERSION COVARIANCE MATRIX:

4.282563658181E+07	-9.308798138141E+04	2.023131415154E+04
-9.308798138141E+04	1.696932409177E+04	-6.360480197909E+03
2.023131415154E+04	-6.360480197909E+03	1.605425422832E+06

One Sigma Uncertainties From Main Diagonal:

6.544129933139E+03	**1.302663582502E+02**	1.267053835806E+03

RELATIVE MONTE CARLO ESTIMATED POSITION DISPERSION COVARIANCE MATRIX:

4.291740970190E+07	-9.389494357188E+04	2.863330763954E+04
-9.389494357188E+04	5.005112964139E+04	-8.108242958814E+03
2.863330763954E+04	-8.108242958814E+03	1.601982277946E+06

One Sigma Uncertainties From Main Diagonal:

6.551138046317E+03	**2.237210978906E+02**	1.265694385682E+03

RELATIVE ANALYTIC TRUE POSITION DISPERSION COVARIANCE MATRIX:

4.552474790435E+07	8.876379130440E+06	9.790509630079E+03
8.876379130440E+06	3.320007211203E+06	5.104268670316E+03
9.790509630079E+03	5.104268670316E+03	8.027127114158E+05

One Sigma Uncertainties From Main Diagonal:

6.747202968961E+03	**1.822088694659E+03**	8.959423594271E+02

RELATIVE MONTE CARLO TOTAL POSITION DISPERSION COVARIANCE MATRIX:

4.540100903208E+07	8.814150151238E+06	4.923212318513E+03
8.814150151238E+06	3.338515525613E+06	-9.839076217119E+03
4.923212318513E+03	-9.839076217119E+03	8.051403937792E+05

One Sigma Uncertainties From Main Diagonal:

6.738027087514E+03	**1.827160508990E+03**	8.972961572297E+02

Table 4.14 True Average Elevation Angle Dispersion Calculated From the Condition Covariance Matrix

Orbit	Elevation Type	Covariance Scale Factor	Average Elevation Error	
			Analytic	Monte Carlo
co-circular	1	25	4.4	6.8
		4	1.8	2.1
		1	0.9	0.9
		6.25E-2	0.2	0.2
co-elliptic	1	1E-2	0.3	0.3
	3	1E-2	0.3	0.3

Table 4.15 True Average Elevation Angle Dispersion Calculated From the Error Vectors

Orbit	Elevation Type	Covariance Scale Factor	Average Elevation Error	
			Analytic	Monte Carlo
co-circular	1	25	5.2	5.1
		4	1.8	1.8
		1	0.9	0.9
		6.25E-2	0.2	0.2
co-elliptic	1	1E-2	0.3	0.3
	3	1E-2	0.3	0.3

CHAPTER 5
CONCLUSION

Future missions to Mars will stretch current theories and practices in mission planning and operations well beyond those used to go to the moon. The goal of this study has been to develop a method for propagating a covariance matrix to a maneuver condition to be used in linear covariance analysis for planning the rendezvous phase of these space missions. With the generalized formulation of a condition transition matrix, an analytic method of propagating an augmented covariance matrix to any scalar, terminal maneuver condition has been presented. This augmented covariance matrix includes navigation errors, dispersions, and time errors for both the chaser and target craft. First, the method was analytically developed, then validated by comparison to a stochastic Monte Carlo simulation for the case of several elevation angle conditions which might be used to trigger an initial rendezvous burn. The key assumption of linearity at the terminal point was substantiated with the same simulation. This chapter will summarize the key results of the simulation in Section 5.1, and suggest some future, related areas for research in Section 5.2.

5.1 Summary of Results

The primary result of this study is a valid analytic method of propagating to a condition. Three important conclusions can be drawn from the results of the comparison of this analytic method with a stochastic Monte Carlo simulation:

- The condition transition matrix, developed in Chapter 2, is a valid analytic means of propagating a covariance matrix to a maneuver condition.
- The assumption of linearity at the terminal point is valid for 'small' initial perturbations.
- For an elevation angle condition, the final estimated state errors at the condition do collapse along the line of sight between the spacecraft.

This section will expand on these three conclusions.

The analytic result (the propagation of an initial augmented covariance matrix to a maneuver condition using a variable time of flight condition transition matrix) was validated, first, by accurately propagating deterministic error vectors to the desired condition. The elevation angle was held constant, and the final state was verified with a separate Kepler propagation to the same perturbed time. The analytic method was then shown to produce the same final condition covariance matrix as that of the stochastic Monte Carlo simulation. In particular, the result was shown for a co-circular orbital case with the elevation angle referenced to the local horizontal, and for a co-elliptic case with the elevation angle referenced to the chaser's velocity vector. Finally, the variation in the elevation angle was calculated from the final condition covariance matrices. This variation was shown to be small,

confirming that the final state had been constrained to the desired condition.

The linearity assumption was validated for 'small' initial perturbations. The definition of small was investigated, and as stated, will be unique to the orbits of the rendezvousing spacecraft. Using the co-circular case and a transformation to a local vertical, curvilinear coordinate system, the effect of the linearity assumption was shown to be an added altitude error in the final dispersions of both craft. Then, by scaling the initial covariance matrix, the linearity assumption was tested for various sized errors. The analytic method proved to accurately calculate the necessary time slip and achieve the desired elevation angle for an initial covariance matrix representing the uncertainty of a ground uplinked shuttle and target state. When these uncertainties were doubled (with a covariance scale factor of 4), the time slip still agreed with the Monte Carlo simulation to within 0.7 seconds, and the average elevation angle error was held to 0.6 degrees. Only for much larger perturbations (covariance scale factor 25), did the linearity assumption start to break down.

A different transformation, to a rotating, line of sight coordinate system, was necessary to show that, when the elevation angle is constrained, the total perturbation perpendicular to the line of sight between the craft will be small. It was shown that, because the LOS frame rotates with time, and time is allowed to vary, a different perturbation vector was needed to account for the rotated LOS frame of the perturbed state relative to the LOS frame of the nominal state. Once this LOS perturbation vector was calculated, its resulting covariance matrix did reveal that the perturbations had collapsed along the line of sight.

The condition transition matrix, developed in Chapter 2, will analytically propagate a covariance matrix to a maneuver condition. This method will prove to be an effective, time saving tool for the covariance analysis necessary to the planning of the rendezvous phase of any future space mission.

5.2 Future Research

As is always the case, there is more work yet to be done than has already been accomplished. Three areas of future research, directly related to the condition transition matrix, suggest themselves.

The definition of what is small, as it relates to the linearity assumption, was investigated for two very general rendezvous orbit profiles, one co-circular and the other co-elliptic. Because the size, shape, position, and relative size and orientation of the rendezvous orbits all influence the altitude error and affect how fast the elevation angle is changing, and, therefore, how large the perturbations can be before the linearity assumption is invalid, more work is needed to define what is small for specific rendezvous scenarios.

If it, then, proves that the size of the anticipated errors and the planned rendezvous profile will necessitate time slips beyond the region of linearity at the terminal point, work might be done to expand this region of linearity. One possibility is to include second order effects in the condition transition matrix. Another possibility would be to go to a classical element formulation (or a more modern non-singular element formulation) which avoids these linearity problems. Unfortunately, element formulations are difficult to deal with, both algorithmically and computationally. However, for some problems, it may be necessary.

The final direct area of research involves the transformations to the LVC and LOS coordinate systems. Both transformations are non-linear, and were, therefore, performed on the individual perturbation vectors after they were propagated by Analytic or Monte Carlo. Covariance matrices were then calculated from these

transformed vectors. An Analytic method for directly transforming the inertial condition covariance matrix should be possible and would further increase the flexibility and value of the condition transition matrix.

Not mentioned yet, are the areas which go beyond, and were listed as motivation for, this study. Armed with an analytic method of propagating a covariance matrix to a maneuver condition, questions related to the Mars highly elliptic rendezvous problem can be more easily addressed. Some of these questions are: the size and shape of the catch-up orbit, where in the orbit the rendezvous should occur and where it should be initiated, what condition to trigger the intercept burn on, the geometry of the final approach to the target, and how to make the rendezvous tolerant to navigation uncertainties. There is, indeed, more work yet to be done.

APPENDIX A

This Appendix contains the results, and a few helpful steps, of differentiating the four elevation angle definitions of Chapter 2 to obtain the elements of k^T, the sensitivity vector.

A.1 Elevation Type 1

For the angle between the line of sight and the local horizontal,

$$\sin\phi_1 = \frac{\Delta r^T r_c}{|\Delta r||r_c|} \tag{A.1}$$

two good first steps are:

$$\Delta r = r_t - r_c$$

$$\frac{\partial \Delta r}{\partial r_c} = -\frac{\partial \Delta r}{\partial r_t} = -I$$

and

$$\Delta r^2 = \Delta r^T \Delta r$$

$$2\Delta r \frac{\partial \Delta r}{\partial r_c} = -2\Delta r^T$$

$$\frac{\partial \Delta r}{\partial r_c} = -\frac{\partial \Delta r}{\partial r_t} = -\frac{\Delta r^T}{|\Delta r|} \tag{A.2}$$

and the result:

$$\frac{\partial \phi_1}{\partial \boldsymbol{r}_c} = \alpha_1 \left[r_c^2 \left(\Delta \boldsymbol{r}^{\mathrm{T}} \boldsymbol{r}_t \right) \Delta \boldsymbol{r}^{\mathrm{T}} - \Delta r^2 \left(\boldsymbol{r}_c^{\mathrm{T}} \boldsymbol{r}_t \right) \boldsymbol{r}_c^{\mathrm{T}} \right] \tag{A.3}$$

$$\frac{\partial \phi_1}{\partial \boldsymbol{v}_c} = \mathbf{0}_3^{\mathrm{T}} \tag{A.4}$$

$$\frac{\partial \phi_1}{\partial \boldsymbol{r}_t} = \alpha_1 r_c^2 \left[\Delta r^2 \boldsymbol{r}_c^{\mathrm{T}} - \left(\Delta \boldsymbol{r}^{\mathrm{T}} \boldsymbol{r}_c \right) \Delta \boldsymbol{r}^{\mathrm{T}} \right] \tag{A.5}$$

where

$$\alpha_1 = \frac{\sec \phi_1}{\Delta r^3 \, r_c^3} \tag{A.6}$$

A.2 Elevation Type 2

When correcting for non-co-planar orbits,

$$\sin\phi_2 = \frac{\Delta r^{\mathrm{T}} r_c}{\left|r_c\right|\left|\Delta r - \frac{1}{h_c^2}(r_t^{\mathrm{T}} h_c) h_c\right|} = \frac{\Delta r^{\mathrm{T}} r_c}{r_c\left[\Delta r^2 - \frac{1}{h_c^2}\left(r_t^{\mathrm{T}} h_c\right)^2\right]^{\frac{1}{2}}} \tag{A.7}$$

a few more helpful steps are needed [1]:

$$h_c = -v_c \times r_c = -S_{v_c} v_c \qquad \text{where} \qquad S_{v_c} = \begin{bmatrix} 0 & -v_z & v_y \\ v_z & 0 & -v_x \\ -v_y & v_x & 0 \end{bmatrix} = -S_{v_c}^{T} \tag{A.8}$$

$$\frac{\partial h_c}{\partial r_c} = -S_{v_c} \quad \Rightarrow \quad \frac{\partial\left(r_t^{\mathrm{T}} h_c\right)}{\partial r_c} = -r_t^{\mathrm{T}} S_{v_c} = \left(-S_{v_c}^{\mathrm{T}} r_t\right)^{\mathrm{T}} = \left(S_{v_c} r_t\right)^{\mathrm{T}} = \left(v_c \times r_t\right)^{\mathrm{T}} \tag{A.9}$$

$$h_c^2 = h_c^{\mathrm{T}} h_c$$

$$2h_c \frac{\partial h_c}{\partial r_c} = 2h_c^{\mathrm{T}} \frac{\partial h_c}{\partial r_c} = -2h_c^{\mathrm{T}} S_{v_c} \tag{A.10}$$

$$\frac{\partial h_c}{\partial r_c} = \frac{\left(-S_{v_c}^{\mathrm{T}} h_c\right)^{\mathrm{T}}}{h_c} = \frac{\left(v_c \times h_c\right)^{\mathrm{T}}}{h_c} = \frac{v_c^2 r_c^{\mathrm{T}} - \left(r_c^{\mathrm{T}} v_c\right) v_c^{\mathrm{T}}}{h_c}$$

Similar results are found in ref. [1] for the partials with respect to the velocity vector.

With a few more steps, the desired partials are:

$$\frac{\partial \phi_2}{\partial r_c} = \alpha_2 \Bigg\{ \left[\frac{1}{h_c^4} \left(r_t^{\mathrm{T}} h_c \right)^2 \left[r_c^2 h_c^2 + \left(\Delta r^{\mathrm{T}} r_c \right) \left(r_c^2 v_c^2 + h_c^2 \right) \right] - \Delta r^2 \left(r_t^{\mathrm{T}} r_c \right) \right] r_c^{\mathrm{T}} + r_c^2 \left[\left(\Delta r^{\mathrm{T}} r_t \right) - \frac{1}{h_c^2} \left(r_t^{\mathrm{T}} h_c \right)^2 \right] \Delta r^{\mathrm{T}} + \frac{r_c^2}{h_c^4} \left(\Delta r^{\mathrm{T}} r_c \right) \left(r_c^{\mathrm{T}} v_c \right) \left(r_t^{\mathrm{T}} h_c \right)^2 v_c^{\mathrm{T}} - \frac{r_c^2}{h_c^2} \left(\Delta r^{\mathrm{T}} r_c \right) \left(r_t^{\mathrm{T}} h_c \right) \left(r_t \times v_c \right)^{\mathrm{T}} \Bigg\} \tag{A.11}$$

$$\frac{\partial \phi_2}{\partial v_c} = \alpha_2 \frac{r_c^2}{h_c^4} \left(\Delta r^{\mathrm{T}} r_c \right) \left(r_t^{\mathrm{T}} h_c \right) \left[\left(r_t^{\mathrm{T}} h_c \right) \left[\left(r_c^{\mathrm{T}} v_c \right) r_c^{\mathrm{T}} - r_c^2 v_c^{\mathrm{T}} \right] - h_c^2 \left(r_c \times r_t \right)^{\mathrm{T}} \right] \tag{A.12}$$

$$\frac{\partial \phi_2}{\partial r_t} = \alpha_2 r_c^2 \left[\left[\Delta r^2 - \frac{1}{h_c^2} \left(r_t^{\mathrm{T}} h_c \right)^2 \right] r_c^{\mathrm{T}} - \left(\Delta r^{\mathrm{T}} r_c \right) \left[\Delta r^{\mathrm{T}} - \frac{1}{h_c^2} \left(r_t^{\mathrm{T}} h_c \right) h_c^{\mathrm{T}} \right] \right] \tag{A.13}$$

where

$$\alpha_2 = \frac{\sec \phi_2}{r_c^3 \left[\Delta r^2 - \frac{1}{h_c^2} \left(r_t^{\mathrm{T}} h_c \right)^2 \right]^{\frac{3}{2}}} \tag{A.14}$$

A.3 Elevation Type 3

The remaining partials for the angle between the line of sight and the velocity vector are derived using the same tools, and are presented without comment.

$$\cos\phi_3 = \frac{\Delta r^T v_c}{|\Delta r||v_c|} \tag{A.15}$$

yields

$$\frac{\partial\phi_3}{\partial r_c} = \alpha_3 v_c^2\left[\left(\Delta r^T v_c\right)\Delta r^T - \Delta r^2 v_c^T\right] \tag{A.16}$$

$$\frac{\partial\phi_3}{\partial v_c} = \alpha_3 \Delta r^2\left[v_c^2 \Delta r^T - \left(\Delta r^T v_c\right)v_c^T\right] \tag{A.17}$$

$$\frac{\partial\phi_3}{\partial r_t} = \alpha_3 v_c^2\left[\Delta r^2 v_c^T - \left(\Delta r^T v_c\right)\Delta r^T\right] \tag{A.18}$$

where

$$\alpha_3 = \frac{-csc\,\phi_3}{\Delta r^3\, v_c^3} \tag{A.19}$$

A.4 Elevation Type 4

$$\begin{aligned}\sin\phi_4 &= \frac{\Delta r^{\mathrm{T}} v_c}{\left|v_c\right|\left|\Delta r - \frac{1}{h_c^2}(r_t^{\mathrm{T}} h_c) h_c\right|} \\ &= \frac{\Delta r^{\mathrm{T}} v_c}{v_c\left[\Delta r^2 - \frac{1}{h_c^2}\left(r_t^{\mathrm{T}} h_c\right)^2\right]^{\frac{1}{2}}}\end{aligned} \tag{A.20}$$

leads to

$$\begin{aligned}\frac{\partial \phi_4}{\partial r_c} = \alpha_4 v_c^2 \Bigg\{ & \left(\Delta r^{\mathrm{T}} v_c\right)\left[\frac{v_c^2}{h_c^4}\left(r_t^{\mathrm{T}} h_c\right)^2 r_c^{\mathrm{T}} + \Delta r^{\mathrm{T}}\right] \\ & + \left[\frac{1}{h_c^4}\left[h_c^2 + \left(\Delta r^{\mathrm{T}} v_c\right)\left(r_c^{\mathrm{T}} v_c\right)\right]\left(r_t^{\mathrm{T}} h_c\right)^2 - \Delta r^2\right] v_c^{\mathrm{T}} \\ & - \frac{1}{h_c^2}\left(\Delta r^{\mathrm{T}} v_c\right)\left(r_t^{\mathrm{T}} h_c\right)\left(r_t \times v_c\right)^{\mathrm{T}} \Bigg\}\end{aligned} \tag{A.21}$$

$$\frac{\partial \phi_4}{\partial v_c} = \alpha_4 \Bigg\{ \frac{v_c^2}{h_c^4}\left(r_t^{\mathrm{T}} h_c\right)^2 \left(\Delta r^{\mathrm{T}} v_c\right)\left(r_c^{\mathrm{T}} v_c\right) r_c^{\mathrm{T}} + v_c^2\left[\Delta r^2 - \frac{1}{h_c^2}\left(r_t^{\mathrm{T}} h_c\right)^2\right]\Delta r^{\mathrm{T}} + \left(\Delta r^{\mathrm{T}} v_c\right)\left[\frac{1}{h_c^4}\left(h_c^2 - r_c^2 v_c^2\right)\left(r_t^{\mathrm{T}} h_c\right)^2 - \Delta r^2\right] v_c^{\mathrm{T}} - \frac{v_c^2}{h_c^2}\left(\Delta r^{\mathrm{T}} v_c\right)\left(r_t^{\mathrm{T}} h_c\right)\left(r_c \times r_t\right)^{\mathrm{T}} \Bigg\} \tag{A.22}$$

$$\frac{\partial \phi_4}{\partial r_t} = \alpha_4 v_c^2 \left[\left[\Delta r^2 - \frac{1}{h_c^2}\left(r_t^{\mathrm{T}} h_c\right)^2\right] v_c^{\mathrm{T}} - \left(\Delta r^{\mathrm{T}} v_c\right)\left[\Delta r^{\mathrm{T}} - \frac{1}{h_c^2}\left(r_t^{\mathrm{T}} h_c\right) h_c^{\mathrm{T}}\right]\right] \tag{A.23}$$

where

$$\alpha_4 = \frac{-csc\,\phi_4}{v_c^3\left[\Delta r^2 - \frac{1}{h_c^2}\left(r_t^{\mathrm{T}} h_c\right)^2\right]^{\frac{3}{2}}} \tag{A.24}$$

BIBLIOGRAPHY

[1] Battin, R. H., *Introduction to the Mathematics and Methods of Astrodynamics*, American Institute of Aeronautics and Astronautics, Inc., New York, N.Y. 1987.

[2] Bottkol, M. S., "Chi-Square Test," Draper Laboratory, Personal Notes.

[3] "Elliptic Orbit Rendezvous Study," Draper Laboratory Interlab Report.

[4] Goss, R. D., and Muller, E. S., "Space Guidance Analysis Memo #56," MIT Instrumentation Laboratory (now Draper Lab), August 13, 1963.

[5] "Guidance, Navigation, and Control; Part A: Guidance, On-Orbit/Deorbit," *Space Shuttle Orbiter, Operational, Level C, Functional Subsystem Software Requirements Document*, STS 83-0003C, Rockwell International, June 18, 1990.

[6] Shepperd, S. W., "Universal Conic State Transition Matrices," Draper Laboratory, Personal Communication.

[7] Shepperd, S. W., "Universal Keplerian State Transition Matrix," *Celestial Mechanics*, Vol. 35, 1985, pp. 129-144.

[8] Suddath, J. H., "Generating Random Vectors for Statistical Studies," NASA Memorandum, EH3-82-036, December 27, 1982.

[9] Tempelman, W., "Linear Guidance Laws for Space Missions," *Journal of Guidance, Control, and Dynamics*, July-August 1986, pp. 495-502.

[10] Tempelman, W., "Properties of Conic State Transition Matrices and Associated Time Partials," *Journal of Guidance, Control, and Dynamics,* Vol. 7, March-April 1984, pp. 135-140.